tially identical results. After treatment with RNase H, cDNA probes were purified by gel filtration. Hybridization and washing of the microarray were carried out according to the manufacturer's instructions. In brief, cDNA probe solutions containing both Cy3- and Cy5-labeled cDNA probes were applied to the microarrays, and the microarrays were covered with a spaced glass cover slip (Takara Bio) and placed in a humidified chamber at 65°C for 16 h. Then, the microarrays were sequentially washed in 2× SSC (150 mM NaCl and 15 mM sodium citrate) containing 0.2% sodium dodecylsulfate (SDS) for 5 min twice at 55°C, in 2× SSC containing 0.2% SDS for 5 min once at 65°C and in 0.05× SSC for 1 min once at room temperature. The microarrays were scanned in both Cy3 and Cy5 channels with a ScanArray Lite (Packard BioChip Technologies, Billerica, MA, USA). QuantArray software (Packard BioChip Technologies) was used for image analysis. Genes were considered to be positively expressed if the signal/background ratio was >3.0. The average of glyceraldehyde 3-phosphate dehydrogenase (G3PDH) Cy3 and Cy5 signals (12 spots each) gave a ratio that was used to balance or normalize the signals.[14–17]

Addition of free radical scavengers

For free radical scavenging, 7.0×10^6 cells were suspended in culture medium containing 0.2 mM of NAC and incubated at 37°C for 1 h. Before sonication, cells were centrifuged and gently resuspended in 4 ml of Ar-saturated medium containing the same scavenger and transferred to a 35-mm culture dish to be sonicated. Cells in a dish were sonicated with 1.0-MHz ultrasound at 1.1 W/cm^2 for 60 s and then incubated at 37.0°C for 7 h after addition of FBS at a concentration of 10%.

Western blotting

Sonicated cells were collected by centrifugation and lysed at room temperature for 15 min in Passive Lysis Buffer (Promega, Madison, WI, USA) after being washed in phosphate-buffered saline (PBS) twice. The protein concentration of the centrifuged supernatant was measured by using a Protein Assay Kit (Nippon Bio-Rad Laboratories, Tokyo, Japan). After the protein concentrations were standardized, each of the cell lysates was mixed with the same volume of 2× SDS loading buffer (200 mM dithiothreitol, 4% SDS, 0.2% bromophenol blue, 20% glycerol, and 100 mM Tris-HCl, pH 6.8) and boiled at 95°C for 10 min. The samples were electrophoresed on 12% polyacrylamide gel and then transferred onto an immobilon PVDF membrane (Nihon Millipore, Tokyo, Japan). After the membrane was blocked in 5% skim milk in PBS, it was treated with an anti-HO-1 polyclonal antibody (Santa Cruz Biotechnology, Santa Cruz, CA, USA) and a secondary antibody conjugated with alkaline phosphatase (Chemicon International, Temecula, CA, USA). The HO-1 protein band was visualized with CDP-Star (Tropix, Bedford, MA, USA) and recorded on a LAS-1000 chemi-luminescence detector (Fuji Photo Film, Tokyo, Japan).

Real-time PCR analysis

Using an RNeasy Total RNA Extraction Kit (Qiagen), whole cell RNA was extracted from 1.4×10^6 cells, following the manufacturer's instructions. cDNA was synthesized by RT reaction at 37°C for 1 h with an Omniscript Reverse Transcription Kit (Qiagen). For the real-time quantitative PCR reaction, HO-1-F (5′-GAGGGAAGCCCCCACTCA-3′) and HO-1-R (5′-AACTGTCGCCACCAGAAAGCT-3′) were used as primers for HO-1 mRNA, and G3PDH-F (5′-AAGGACTCATGACCACAGTCCAT-3′) and G3PDH-R (5′-CCATCACGCCACAGTTTCC-3′) were used as primers for the inner control, G3PDH. As TaqMan probes, we used HO-1-T (5′-CCGCTCCCAGGCTCCGC TTC-3′) and G3PDH-T (5′-CCATCACTGCCACCCA-GAAGACTGTG-3′) for HO-1 and G3PDH, respectively. The probes were labeled with FAM for the 5′ end and TAMRA for the 3′ end. The reaction mixture, which comprised 1 μg of cDNA, 900 nM of each primer, 200 nM of each TaqMan probe, qPCR Mastermix (Nippon Gene Co., Toyama, Japan), and 5 mM of $MgCl_2$, was used in an ABI Prism 7700 sequence detection system (Applied Biosystems, Foster, CA) for reactions of 40 cycles at 95.0°C for 15 s and at 60.0°C for 60 s preceded by reactions at 50.0°C for 2 min and 95.0°C for 10 min. The ratio of HO-1 inductions was calculated by the following formula: $Y = X_U/X_0$, where X_U is the signal ratio of HO-1 to G3PDH in a sample with sonication and X_0 is the signal ratio of HO-1 to G3PDH in a sample without sonication.

Detection of mitochondrial transmembrane potential and intracellular superoxide formation

We used $DiOC_6(3)$ and HE for detecting the mitochondrial transmembrane potential and intracellular superoxide formation, respectively. After exposure to ultrasound, the cells were incubated for 6 h and collected by centrifugation at 1000× *g* for 3 min. The cells (approximately 1×10^6 cells) were resuspended in PBS containing 1% FBS, and 40 nM $DiOC_6(3)$ or 2 μM HE. They were then incubated at 37°C for 15 min and washed twice in PBS before flow cytometric analysis (FACSCalibur, Nippon Becton Dickinson, Tokyo, Japan).

Statistical analysis

All values are expressed as mean ± standard deviation (SD). Differences were assessed by using Student's unpaired *t* test. Statistical significance was established at a value of $P < 0.01$.

22

Table 1. Up- and downregulated genes after sonication in U937 cells

Gene	Fold change			GenBank accession no.
	Exp. 1	Exp. 2	Average	
Upregulated				
PCTAIRE protein kinase 1 Transcript variant 2 (PCTK1-V2)	2.5	2.1	2.3	NM_033018
Heme oxygenase-1 (HO-1)	3.4	2.4	2.9	NM_002133
Downregulated				
Leukemia inhibitory factor receptor (LIFR)	0.17	0.23	0.20	NM_002310
Chemokine ligand 10 (CXCL10)	0.50	0.43	0.47	NM_001565

Microarray analysis was performed (details of experimental conditions are described in the materials and methods section)
Exp., experiment

Results

cDNA microarray analysis

In order to identify genes that are differentially expressed in U937 cells treated with ultrasound for 1 min at an intensity of 3.6 W/cm², we carried out cDNA microarray analysis of the cells 6 h after ultrasound treatment. Hydroxyl radical formation, the fraction of intact cells, and apoptosis under these experimental conditions have been described in previous reports.[7,17] Genes were considered to be up- or downregulated if the average fold change was 2.0 or greater in duplicate experiments. Of the 3893 genes examined, changes in mRNA levels were detected in four genes: two genes, PCTAIRE protein kinase 1 transcript variant 2 (*PCTK1-V2*) and *HO-1*, were upregulated, whereas two genes, leukemia inhibitory factor receptor (*LIFR*) and chemokine ligand 10 (*CXCL10*), were downregulated by ultrasound treatment. The average fold change of *PCTK1-V2, HO-1, LIFR* and *CXCL10* was 2.3, 2.8, 0.20, and 0.47, respectively (Table 1). Thus, upregulation of *HO-1* was confirmed, and three genes responding to ultrasonic cavitation were identified.

9

Cell survival and free radical formation

When the U937 cells were sonicated for 1 min with graded intensity, the survival rate decreased with increasing intensity except at intensities less than 0.3 W/cm². Furthermore, the relationship between ultrasonic intensity and hydroxyl radical formation, which is an endpoint of inertial cavitation, was studied with EPR spin trapping using DMPO as a spin trap. In a similar manner, the EPR signal of DMPO-OH adducts was not detected at up to 0.3 W/cm², and it increased with increasing intensity up to 1.4 W/cm² (Fig. 1a). At an intensity of 1.6 W/cm², formation of DMPO-OH adduct decreased. The reason or reasons for the decrease are unknown. However, it could be attributed to a rapid degassing effect at high intensity or premature collapse of cavitation at intensities much greater than the threshold of cavitation, meaning that the bubbles cannot gain enough energy from the momentum of oscillation.

Dose response of HO-1 induction

10

When the U937 cells were sonicated for 1 min at graded intensities, HO-1 expression was examined by Western blotting after 7 h. The level of expression increased with increasing intensity up to 1.4 W/cm² (Fig. 1b). Furthermore, the effects of incubation time on HO-1 expression were examined in cells exposed to ultrasound at 1.1 W/cm². HO-1 expression increased with increasing incubation time up to 7 h (Fig. 1c).

Effects of NAC

To verify the involvement of reactive oxygen species (ROS), we sonicated cells with or without NAC, a broad-range scavenger of ROS, and measured HO-1 expression by using real-time quantitative PCR. As shown in Fig. 2, the fold induction of HO-1 expression in the sonicated samples without NAC was 25.7 ± 11.2 (mean ± SD; n = 21), whereas that of sonicated samples in the presence of 200 μM NAC was 2.2 ± 0.7 (mean ± SD; n = 4). This showed that addition of NAC suppressed the induction of HO-1 expression, affirming the role of ROS. In addition, even when NAC was added immediately after sonication, HO-1 induction was still suppressed in a manner comparable to that observed in cells treated with NAC before sonication (mean ± SD 2.2 ± 0.6; n = 3), suggesting the involvement of ROS generated intracellularly after sonication or the formation of ROS with long half-lives such as hydrogen peroxide.

11

Change in mitochondrial transmembrane potential and superoxide formation

To examine the source of ROS involved in HO-1 induction, change in mitochondrial transmembrane potential and

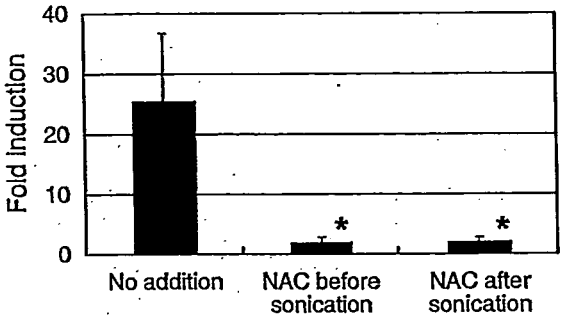

Fig. 2. Effects of an antioxidant, *N*-acetyl-l-cysteine (NAC), on HO-1 expression induced by ultrasound. U937 cells were pre-incubated in medium containing 0.2 mM of NAC for 1 h and then sonicated for 60 s with 1.0-MHz continuous wave at 1.1 W/cm², or were treated with NAC immediately after sonication and incubated for 7 h. HO-1 expression was examined by real-time quantitative PCR. The ratio of HO-1 induction to that in a sample without sonication was determined and expressed as fold induction. The error *bars* in the figure are the standard deviations ($n = 3$). *Asterisks* indicate a statistically significant difference relative to ■■ ($P < 0.01$)

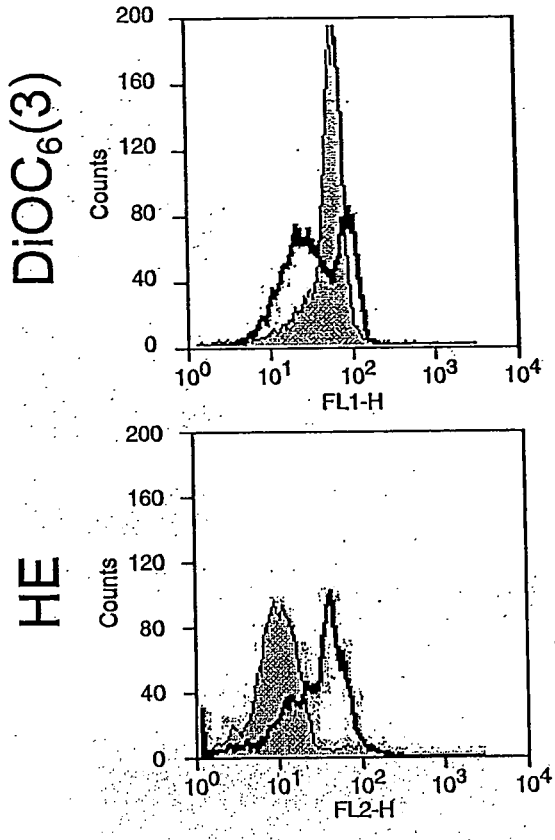

Fig. 3. Change in mitochondrial transmembrane potential and generation of intracellular superoxide after sonication. U937 cells were sonicated for 60 s with 1.0-MHz continuous wave at 1.1 W/cm². The cells were harvested 6 h after sonication and stained with 40-nM $DiOC_6(3)$ or 2-mM HE for flow cytometric analysis. The *gray area* shows the distribution of cells without sonication and the *solid line* shows that of the sonicated cells

superoxide formation was estimated by using the fluorescent probes $DiOC_6(3)$ and HE, respectively. For measurement of mitochondrial transmembrane potential, the fraction (%) of cells with low mitochondrial transmembrane potential in control samples was 9.3 ± 15.1 (mean ± SD, $n = 3$). However, that of sonicated samples was 46.1 ± 5.6 (mean ± SD, $n = 3$) 6 h after sonication (Fig. 3). Similarly, the fraction (%) of cells with superoxide formation in control samples was 7.2 ± 2.6 (mean ± SD, $n = 3$), whereas that in sonicated samples was 66.3 ± 1.2 (mean ± SD, $n = 3$) 6 h after sonication (Fig. 3). These results clearly indicate mitochondrial dysfunction and superoxide formation in the sonicated cells.

HO-1 induction in a variety of cell lines

To obtain comprehensive data on HO-1 induction by ultrasound, human prostatic cancer cell lines (DU145 and LNCap), human leukemia cell lines (Jurkat and K562) and a mouse leukemic monocyte cell line (RAW 264) were also used. These five kinds of cells were sonicated for 1 min with an intensity of 1.1 W/cm², and HO-1 protein expression was examined after 7 h. HO-1 was clearly induced in DU145 and Jurkat cells, but not in the others (Fig. 4).

HO-1 induction by H_2O_2, Cd, and X-irradiation

The U937 cells were treated with H_2O_2 at a concentration of 600 μM, and with $CdCl_2$ at a concentration of 5 μM, for 6 h, after which they were harvested for Western blotting. Both agents clearly induced the protein expression of HO-1 in U937 cells (Fig. 5a). X-irradiation also induced expression depending on the radiation dose. These results indicate that oxidative stress, H_2O_2, Cd ions, and X-irradiation induce HO-1 in U937 cells (Fig. 5b).

Discussion

Previously, using cDNA microarray and semi-quantitative RT-PCR techniques, we analyzed changes in the gene expression of U937 cells in a medium saturated with Ar after sonication with a 1.0-MHz continuous wave. We found that the *HO-1* gene was related to the cavitation-mediated mechanism and was upregulated 6.6-fold, which was the highest upregulation among the genes investigated.[17] In the present study, first we used a cDNA microarray system to confirm and discover new genes that respond to ultrasonic cavitation. Second, we used real-time quantitative PCR and Western blotting techniques to explore the mechanism of *HO-1* upregulation. The results reconfirmed *HO-1* upregu-

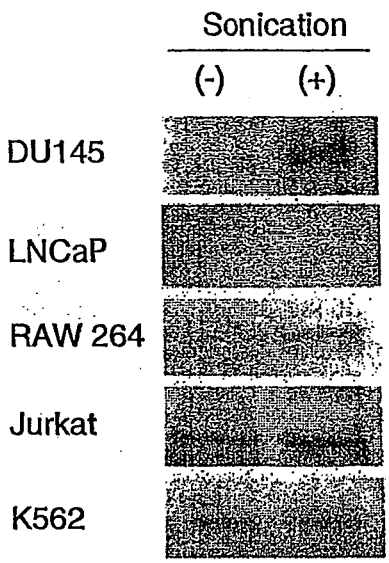

Fig. 4. Western blot analysis of HO-1 in five cell lines. The cells were sonicated for 60 s with 1.0-MHz continuous wave at 1.1 W/cm² and harvested 7 h after sonication

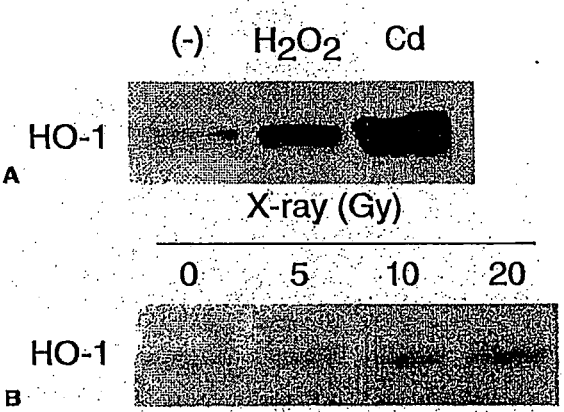

Fig. 5. Western blot analysis of HO-1 in U937 cells. a Cells treated with H_2O_2 (600 μM) or with $CdCl_2$ (5 μM). The cells were treated with H_2O_2 or $CdCl_2$ for 6 h and then harvested for Western blotting. b Cells exposed to X-rays at 5, 10, and 20 Gy. After X-irradiation, the cells were incubated for 6 h and harvested for Western blotting

lation, and *PCTK1-V2* was identified as another upregulated gene. Two other genes, *LIFR* and *CXCL10*, were found to be downregulated. In addition, the data suggest that O_2^- secondarily generated in damaged mitochondria resulting from sonomechanical effects gives rise to intracellular oxidative stress to induce *HO-1* expression.

HO is an enzyme-catalyzing heme, which coordinately bonds to oxygen in the living body as a prosthetic group of hemoglobin or cytochrome p-450, Fe^{2+}, carbon monoxide and biliverdin. Biliverdin is subsequently converted to bilirubin in the cytosol by biliverdin reductase. HO is considered a rate-limiting enzyme in the process of heme catabolism.[19] HO consists of three isozymes: HO-1, HO-2 and HO-3.[20] HO-1 has been extensively studied. It is an isozyme induced by metal ions, such as cadmium[21,22] and cobalt,[23] and by physical and chemical stresses such as treatment with 12-o-tetradecanoylphorbol 13-acetate,[24] ultraviolet light,[25] hydrogen peroxide[25] and donors of nitric oxide.[26] In addition, oxidative stress caused by ischemia-reperfusion injury is known to induce HO-1.[27] It has been reported that HO-1-deficient embryonic fibroblasts are hypersensitive to both hemin and hydrogen peroxide cytotoxicity, as supported by genetic evidence that upregulation of HO-1 serves as an adaptive mechanism to protect cells from oxidative damage during stress.[28] However, the mechanism by which HO-1 is induced by ultrasound, a form of mechanical stress, has not yet been elucidated.

Bioeffects of ultrasound occur because of thermal and nonthermal effects. The latter are further classified into cavitational and noncavitational effects. Cavitation is known to lead to both mechanical shear stress and/or shock waves (mechanical effects) and free radical formation (an example of chemical effects) arising from the collapse of oscillating bubbles. Because upregulation of HO-1 was observed at intensities greater than 0.8 W/cm² in the present study, where a significant decrease in cell survival rate and apparent free radical production were observed, upregulation of HO-1 is likely to be cavitation-related. The next question is whether the upregulation is caused by the mechanical effects or the chemical effects associated with cavitation.

To answer this question, we sonicated cells with or without NAC, which is a potent antioxidant, and measured HO-1 expression by using real-time quantitative PCR. As shown in the results, even when NAC was added immediately after sonication, HO-1 induction was significantly suppressed, suggesting that HO-1 induction is most likely due to intracellularly generated ROS after sonication because the addition of culture medium sonicated at 1.1 W/cm² even for 5 min did not induce HO-1 in this cell line (the mean (±SD) fold induction was 1.2 ± 0.8 (n = 4)). Interestingly, our previous data have shown that the addition of NAC after sonication also increased intracellular glutathione concentration and suppressed apoptosis, but did not affect intracellular superoxide formation or mitochondrial transmembrane potential.[9] Restored intracellular glutathione appears to scavenge a variety of peroxides to reduce the intracellular oxidative stress and suppress HO-1 induction and apoptosis without affecting superoxide formation and mitochondrial function. Data on HO-1 induction in a variety of cell lines suggest that HO-1 induction by ultrasound appears to be a cell line-specific event. Ultrasound induced HO-1 in the U937 and Jurkat human leukemia cell lines, but not in the K562 cell line. Not only ultrasound, but also other oxidative stresses, including H_2O_2, $CdCl_2$ and X-irradiation, were able to induce HO-1 in U937 cells. We have shown that these stresses also induce apoptosis in this cell line.[29-31]

Recently, the enhancement of ischemia-reperfusion-induced lung apoptosis by inhibition of HO-1 using a

siRNA technique has been reported.[32] We have already reported apoptosis induced by ultrasound in human lymphoma cell lines, and discovered that the apoptosis is due to an increase in intracellular oxidative stress and intracellular free calcium ions.[9] Therefore, the elucidation of intracellular oxidative stress-mediated interactions between apoptosis and HO-1 induced by ultrasound remains a subject for future studies.

Conclusion

We used a cDNA microarray system to confirm the identity of known genes and discover new genes that respond to ultrasonic cavitation. We confirmed upregulation of the *HO-1* gene and further identified one upregulated and two downregulated genes. In addition, we suggest that increased intracellular oxidative stress secondary to sonomechanical effects arising from ultrasonic cavitation is a potential mechanism of enhancement of HO-1 expression.

Acknowledgment This study was supported by the Research and Development Committee Program of the Japan Society of Ultrasonics in Medicine.

References

1. Feril LB Jr, Kondo T, Umemura S, et al. Sound waves and antineoplastic drugs: The possibility of an enhanced combined anticancer. J Med Ultrasonics 2000;29:173–87.
2. Feril LB Jr, Kondo T. Biological effects of low intensity ultrasound: The mechanism involved, and its implications on therapy and on biosafety of ultrasound. J Radiat Res 2004;45:479–89.
3. Henglein A. Sonochemistry: Historical developments and modern aspects. Ultrasonics 1987;25:6–16.
4. Suslick KS. Sonochemistry. Science 1990;247:1439–45.
5. Riesz P, Kondo T. Free radical formation induced by ultrasound and its biological implications. Free Radic Biol Med 1992;13: 247–70.
6. Ashush H, Rozenszajn LA, Blass M, et al. Apoptosis induction of human myeloid leukemic cells by ultrasound exposure. Cancer Res 2000;60:1014–20.
7. Honda H, Zhao QL, Kondo T. Effects of dissolved gases and an echo contrast agent on apoptosis induced by ultrasound and its mechanism via the mitochondoria-caspase pathway. Ultrasound Med Biol 2002;28:673–82.
8. Feril LB Jr, Kondo T, Zhao Q-L, et al. Enhancement of ultrasound apoptosis and cell lysis by echo-contrast agents. Ultrasound Med Biol 2003;29:331–7.
9. Honda H, Kondo T, Zhao QL, et al. Role of intracellular calcium ions and reactive oxygen species in apoptosis induced by ultrasound. Ultrasound Med Biol 2004;30:683–92.
10. Feril LB Jr, Kondo T, Takaya K, et al. Enhanced ultrasound-induced apoptosis and cell lysis by a hypotonic medium. Int J Radiat Biol 2004;80:165–75.
11. Feril LB Jr, Kondo T, Cui Z-G, et al. Apoptosis induced by the sonomechanical effects of low intensity pulsed ultrasound in a human leukemia cell line. Cancer Lett 2005;221:145–52.
12. Cheung VG, Morley M, Aguilar F, et al. Making and reading microarrays. Nat Genet 1999;21(Suppl 1):15–19.
13. Schena M, Shalon D, Davis RW, et al. Quantitative monitoring of gene expression patterns with a complementary DNA microarray. Science 1995;270:467–70.
14. Tabuchi Y, Kondo T. cDNA microarray analysis reveals chop-10 plays a key role in Sertoli cell death induced by bisphenol A. Biochem Biophys Res Commun 2003;305:54–61.
15. Hirano H, Tabuchi Y, Kondo T, et al. Analysis of gene expression in apoptosis of human lymphoma U937 cells induced by heat shock and the effects of α-phenyl N-tert-butylnitrone (PBN) and its derivatives. Apoptosis 2005;10:331–40. 15
16. Tabuchi Y, Kondo T, Suzuki Y, et al. Genes involved in nonpermissive temperature-induced cell differentiation in Sertoli TTE3 cells bearing temperature-sensitive simian virus 40 large T-antigen. Biochem Biophys Res Commun 2005;329:947–56.
17. Tabuchi Y, Kondo T, Ogawa R, et al. DNA microarray analysis of genes elicited by ultrasound in human U937 cells. Biochem Biophys Res Commun 2002;290:498–503.
18. Kondo T, Kano E. Effect of free radicals induced by ultrasonic cavitation on cell killing. Int J Radiat Biol 1988;54:475–86. 16 17
19. Maines MD. ■■. In: ■■ (eds) Heme oxygenase: clinical applications and function. Boca Raton: CRC Press; 1992. p. 145–201.
20. Maines MD. The heme oxygenase system: a regulator of second messenger gases. Annu Rev Pharmacol Toxicol 1997;37:517–54.
21. Alam J, Shibahara S, Smith A. Transcriptional activation of the heme oxygenase gene by heme and cadmium in mouse hepatoma cells. J Biol Chem 1989;264:6371–5.
22. Alam J, Wicks C, Stewart D, et al. Mechanism of heme oxygenase-1 gene activation by cadmium in MCF-7 mammary epithelial cells. Role of p38 kinase and Nrf2 transcription factor. J Biol Chem 2000;275:27694–702.
23. Gong P, Hu B, Stewart D, et al. Cobalt induces heme oxygenase-1 expression by a hypoxia-inducible factor-independent mechanism in Chinese hamster ovary cells: regulation by Nrf2 and MafG transcription factors. J Biol Chem 2001;276:27018–25.
24. Muraosa Y, Shibahara S. Identification of a cis-regulatory element and putative trans-acting factors responsible for 12-O-tetradecanoylphorbol-13-acetate (TPA)-mediated induction of heme oxygenase expression in myelomonocytic cell lines. Mol Cell Biol 1993;13:7881–91.
25. Keyse SM, Tyrrell RM. Heme oxygenase is the major 32-kDa stress protein induced in human skin fibroblasts by UVA radiation, hydrogen peroxide, and sodium arsenite. Proc Natl Acad Sci USA 1989;86:99–103.
26. Immenschuh S, Tan M, Ramadori G. Nitric oxide mediates the lipopolysaccharide dependent upregulation of the heme oxygenase-1 gene expression in cultured rat Kupffer cells. J Hepatol 1999;30:61–9.
27. Vulapalli SR, Chen Z, Chua BH, et al. Cardioselective overexpression of HO-1 prevents I/R-induced cardiac dysfunction and apoptosis. Am J Physiol Heart Circ Physiol 2002;283:H688–94.
28. Poss KD, Tonegawa S. Reduced stress defense in heme oxygenase 1-deficient cells. Proc Natl Acad Sci USA 1997;94:10925–30.
29. Lin M, Kondo T, Zhao QL, et al. Apoptosis induced by cadmium in human lymphoma U937 cells through Ca^{2+}-calpain and caspase-mitochondria-dependent pathways. J Biol Chem 2000;275:39702–9.
30. Cui ZG, Kondo T, Ogawa R, et al. Enhancement of radiation-induced apoptosis by 6-formylpterin. Free Radical Res 2004;38: 363–73.
31. Cui ZG, Kondo T, Feril LB Jr, et al. Effects of antioxidants on X-ray- or hyperthermia-induced apoptosis in human lymphoma U937 cells. Apoptosis 2004;9:757–63.
32. Zhang X, Shan P, Jiang D, et al. Small interfering RNA targeting heme oxygenase-1 enhances ischemia-reperfusion-induced lung apoptosis. J Biol Chem 2004;279:10677–84.

Available online at www.sciencedirect.com
SCIENCE DIRECT
ELSEVIER
Cancer Letters xx (2006) 1–8
CANCER Letters
www.elsevier.com/locate/canlet

Identification of genes responsive to low intensity pulsed ultrasound in a human leukemia cell line Molt-4

Yoshiaki Tabuchi [a,*], Hidetaka Ando [c], Ichiro Takasaki [a], Loreto B. Feril Jr [b,e], Qing-Li Zhao [b], Ryohei Ogawa [b], Nobuki Kudo [d], Katsuro Tachibana [e], Takashi Kondo [b]

[a] *Division of Molecular Genetics, Life Science Research Center, University of Toyama, 2630 Sugitani, Toyama 930-0194, Japan*
[b] *Department of Radiological Sciences, Faculty of Medicine, University of Toyama, Toyama 930-0194, Japan*
[c] *First Department of Surgery, Faculty of Medicine, University of Toyama, Toyama 930-0194, Japan*
[d] *Laboratory of Biomedical Instrumentation and Measurement, Graduate School of Information Science and Technology, Hokkaido University, Sapporo 060-0814, Japan*
[e] *Department of Anatomy, Fukuoka University School of Medicine, Fukuoka 814-0180, Japan*

Received 20 December 2005; received in revised form 15 February 2006; accepted 15 February 2006

Abstract

We examined the gene expression of human leukemia Molt-4 cells treated with non-thermal low intensity pulsed ultrasound. Six hours after 0.3 W/cm^2 pulsed ultrasound treatment, apoptosis (24±3.3%, mean±SD) with minimal cell lysis was observed. Of approximately 16,600 genes analyzed, BCL2-associated athanogene 3 (*BAG3*), DnaJ (Hsp40) homolog, subfamily B, member 1 (*DNAJB1*), heat shock 70 kDa protein 1B (*HSPA1B*), and heat shock 70 kDa protein 6 (*HSPA6*) showed increased levels of expression while isopentenyl-diphosphate delta isomerase (*IDI1*) and 3-hydroxy-3-methylglutaryl–coenzyme A synthase 1 (*HMGCS1*) showed decreased levels in the cells 3 h after the ultrasound treatment. The expression levels of these six genes were confirmed by a real-time quantitative polymerase chain reaction. To our knowledge, this is the first report of DNA microarray analysis of genes that are differentially expressed in response to apoptosis induced by non-thermal low intensity pulsed ultrasound in human leukemia cells. The present results will provide a basis for further understanding of the molecular mechanisms of effects of not only low intensity pulsed ultrasound but also that of mechanical shear stress in the cells.

Keywords: DNA microarray; Gene expression; Low intensity pulsed ultrasound

1. Introduction

In many medical fields, ultrasound (US) has been widely used for diagnosis and therapy. Biophysical actions of US are divided into three modes, thermal, cavitational and non-thermal non-cavitational effects. Cavitation is known to lead to both mechanical shear stress and free radical formation arising from the oscillation and collapse of cavitation bubbles [1–3]. In general, these two effects (mechanical shear stress and free radicals) of cavitation have been inferred to act simultaneously on all of biological materials. It is well known that fairly intense US induces cell killing, cell lysis, loss of viability and loss of clonogenicity [2]. Currently, of particular interest is its ability to induce apoptosis in human leukemia cell lines [4–12]. Different factors that can influence apoptosis were cited. Among them were, sonochemical mechanism [12], cavitation-mediated enhancement of intracellular calcium ion concentration, intracellular free radical

* Corresponding author. Tel.: +81 76 434 7187; fax: +81 76 434 5176.
E-mail address: ytabu@cts.u-toyama.ac.jp (Y. Tabuchi).

0304-3835/$ - see front matter © 2006 Elsevier Ireland Ltd. All rights reserved.
doi:10.1016/j.canlet.2006.02.011

formation due to mitochondrial membrane damage and free radical formation [10,11], and sonomechanical mechanism [9].

It has been indicated that DNA microarrays are one of the most powerful technologies for functional genomics as it can simultaneously analyze the expression levels of many 100s or many 1000s of genes [13,14]. Recently, we applied DNA microarray technologies to analyze gene expression in cellular differentiation [15] and in a variety of biological responses to physical and chemical stresses, such as sodium butyrate [16], bisphenol A [17,18] and hyperthermia [19]. In our previous study, using UniGEMV Ver2.0 human gene expression microarrays to detect approximately 9200 genes, five up-regulated genes and two down-regulated genes were identified in the human lymphoma U937 cells at 6 h after exposure of fairly intense continuous waves (1 MHz, 4.9 W/cm^2, for 1 min), where not only free radical formation, but also cell lysis and apoptosis were significantly observed [20]. Moreover, under nearly same condition in U937 cells, another microarray system and real-time quantitative polymerase chain reaction (PCR) confirmed up-regulation of heme oxygenase-1 (HO-1) and revealed that HO-1 is the most sensitive gene for US in U937 cells [21]. More recently, following a report by Lagneaux et al. [12], we also reported that non-thermal low intensity pulsed US treatment (1 MHz, 0.3 W/cm^2, 1 min) induced apoptosis in human leukemia cell lines such as U937, Jurkat and Molt-4, and it was revealed that the up-regulation of HO-1 was observed above apoptosis-inducing intensities [9,22]. However, the knowledge of the details of molecular signaling in response to mechanical pressure or pressure waves such as US, particularly low intensity pulsed waves, remains elusive.

In the present study, the gene expression of human leukemia Molt-4 cells treated with low intensity pulsed US were examined by using high-density IntelliGene HS human Expression microarrays to detect approximately 16,600 genes.

2. Materials and methods

2.1. Cell culture

Molt-4 human leukemia cells were obtained from Japanese Cancer Research Resource Bank (Tokyo, Japan). The cells were grown in RPMI 1640 medium (Invitrogen Co., Tokyo, Japan) supplemented with 10% fetal bovine serum (Invitrogen Co.) at 37 °C in humidified air with 5% CO_2.

2.2. US apparatus and intensity measurement

The ultrasonic apparatus (Sonicmaster ES-2, OG Giken Co. Ltd, Okayama, Japan) with a resonant frequency of 1 MHz with 100 Hz pulse repetition frequency (PRF) was used in all the sonication experiments. This device is equipped with a built-in digital timer, intensity regulator, and duty factor (DF) controller. For the sonication procedure, the transducer with a diameter of 5 cm was fixed with a clamp attached to a metal stand to keep the transducer facing directly upward (Fig. 1). We used such near acoustic field produced by the liquid–air interface and did not reduce the standing waves because of the effective occurrence of cavitation.

The spatial-average–temporal-average intensities (ISATA) at 10% DF corresponding to the reading output intensity were measured using an ultrasonic power meter (PM-DT-10E, Ohmic instrument Co., Easton, MD). The peak acoustic amplitude in degassed water was also measured at the distance of 5 cm from the transducer with a calibrated poly-(vinyledene difluoride–trifluoroethylene) needle-type hydrophone, 0.5 mm in diameter (Toray techno Co., Ltd, Shiga, Japan) connected to a PC/AT compatible computer and a digitizing oscilloscope (TDS3034, Tektronix Japan, Ltd, Tokyo, Japan). The ISATA and the peak acoustic pressures corresponding to the reading output of 0.1, 0.2, 0.3, 0.4 and 0.5 W/cm^2 (device-indicated) were 0.048, 0.072, 0.081, 0.092 and 0.105 W/cm^2, and 0.061, 0.105, 0.132, 0.144 and 0.146 MPa, respectively. In this paper we used device-indicated intensities to refer to these values.

For most of the experiments, 0.3 W/cm^2 was used. During such an ultrasonic exposure experiment the change in absorbance of 2 ml of aqueous air-saturated ferrous (Fricke) dosimeter solution after 5 min exposure at 304 nm was 0.0082 ± 0.0015 (mean $\pm$ SD, $n=4$) in a 1 cm path length quartz cell. This dosimeter monitors the extent of the cavitational activity induced by ultrasound by measuring the sum of H_2O_2, OH radicals, and H atoms available to react with ferrous ions.

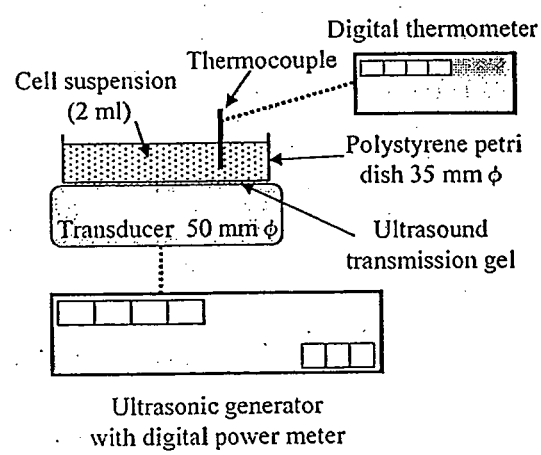

Fig. 1. A set-up for ultrasonic exposure.

2.3. Sonication procedure

The cell concentration used in the experiments was about 2.0×10^6 cells/ml. The cells were gently mixed to homogenize and 1 ml/sample of cell suspension was transferred to a 3 cm polyethylene culture dish. Just before sonication, 1 ml culture medium was added to the cell suspension after gentle shaking. After sonication, the cells were incubated in humidified air with 5% CO_2 at 37 °C for an indicated period before evaluation of DNA fragmentation and other parameters.

2.4. Measurement of cell viability

Trypan blue dye exclusion test was performed. In short, cell suspension was mixed with an equal amount of 0.3% Trypan blue solution (Sigma–Aldrich Co., St Louis, MO) in phosphate-buffered saline. After 5 min incubation at room temperature, the number of cells excluding Trypan blue (unstained) was counted using a Burker Turk hemocytometer to estimate the number of intact viable cells and the number of non-viable cells.

2.5. DNA fragmentation assay

The amount of DNA extracted from cells that had undergone DNA fragmentation was assayed using the method of Sellins and Cohen [23] with a few modifications. Briefly, cells were lysed in lysis buffer (1 mM EDTA, 0.2% Triton X-100 and 10 mM Tris–HCl, pH 7.5) and centrifuged at 13,000 g for 10 min. Subsequently, each DNA sample in the supernatant and the resulting pellet were precipitated in 12.5% trichloroacetic acid (TCA) at 4 °C, and quantified using the diphenylamine reagent after hydrolysis in 5% TCA at 90 °C for 20 min. The percentage of fragmented DNA for each sample was calculated as the amount of DNA in the supernatant divided by the total DNA for that sample (supernatant plus pellet).

2.6. Electron paramagnetic resonance (EPR)-spin trapping for the detection of free radical formation

In this study, we used EPR-spin trapping with 5,5-dimethyl-1-pyrroline-*N*-oxide (DMPO) to detect the US-induced hydroxyl radical formation [2,24]. The cells suspended in culture medium with 10 mM of DMPO were sonicated at 0–0.5 W/cm^2 of 1 MHz 10% DF for 1 min. At 9.425 GHz with a field modulation of 0.1 mT amplitude using a microwave power of 4 mW, EPR spectra of the sonicated solution in a capillary tube were recorded with EPR spectrometer (RFR-30, Radical Research Inc., Tokyo, Japan) at room temperature. The yields of spin adducts were determined using a stable nitroxide radical, TEMPOL (4-hydroxy-2,2,6,6-tetramethyl-1-piperidinyloxy) as a standard. A calibration curve was determined by plotting the product of the peak-to-peak derivative amplitude and the square of the width at maximum slope of the signal versus the different concentrations of the standard nitroxide radical. One unit of the *Y*-axis labeled 'DMPO-OH adduct' is calculated to correspond to about 19.0 μM of TEMPOL.

2.7. Separation of total RNA and mRNA

Total RNA was extracted from the cells using an RNeasy Total RNA Extraction Kit (Qiagen K.K., Tokyo, Japan). Then, RNA samples were treated with RNase-free DNase (Qiagen K.K.) for 30 min at room temperature. mRNAs were extracted from the DNase-treated samples using an Oligotex-dT30 mRNA Purification Kit (Takara Bio Inc., Shiga, Japan).

2.8. cDNA microarray analysis

cDNA microarray analysis was performed by IntelliGene HS human Expression glass microarrays (Takara Bio Inc.), which were spotted with approximately 16,600 cDNA fragments of human genes. A list of these genes is available at Takara's Web site (http://www.takara-bio.co.jp/). Antisense RNA (aRNA) labeled with Cy3 (control group) or Cy5 (treated group) from mRNAs from cells at 3 h after US treatment (for 1 min at 0.3 W/cm^2) by using an RNA Transcript SureLABEL Core Kit (Takara Bio Inc.). In some experiments, control sample was labeled with Cy5; and in others, it was labeled with Cy3, with essentially identical results. Hybridization and washing of the microarray were carried out according to the manufacturer's instructions. In brief, aRNA probe solutions containing both Cy3- and Cy5-labeled aRNA probes were applied to the microarrays, and the microarrays were covered with a spaced glass cover slip (Takara Bio Inc.) and placed in a humidified chamber at 70 °C for 16 h with gentle shaking. Then, the microarrays were sequentially washed in 2× SSC (150 mM NaCl and 15 mM sodium citrate) containing 0.2% SDS for 10 min three times at 65 °C and in 0.05× SSC for 1 min once at room temperature. The microarrays were scanned in both Cy3 and Cy5 channels with a ScanArray Lite (Packard BioChip Technologies, Billerica, MA, USA). QuantArray software (Packard BioChip Technologies) was used for image analysis. Genes were considered to be positive-expressed if the signal/background ratio was >2.0. The average of RPS27A (ribosomal protein S27a, an internal control gene) Cy3 and Cy5 signal (12 spots each) gives a ratio that was used to balance or normalize the signals.

2.9. Real-time quantitative PCR assay

Real-time quantitative PCR was performed on a Real-Time PCR system (Mx3000P, Stratagene Japan K.K., Tokyo, Japan) using Brilliant SYBR Green qPCR Master Mix (Stratagene Japan K.K.) according to the manufacturer's protocol. Reverse transcriptase reaction (Omniscript Reverse Transcriptase, Qiagen K.K.) was carried out with DNase-treated total RNA by using an oligo $d(T)_6$ primer. Real-time

Table 1
Nucleotide sequences of primers for target genes

Genes	Orientation	Nucleotide sequence (position)	GenBank accession no.
HSPA1B	Sense	5′-AGGTGCAGGTGAGCTACAAG-3′ (509–528)	NM_005346
	Antisense	5′-ATGATCCGCAGCACGTTGAG-3′ (722–703)	
BAG3	Sense	5′-CGACCAGGCTACATTCCCAT-3′ (574–593)	NM_004281
	Antisense	5′-TCTGGCTGAGTGGTTTCTGG-3′ (749–730)	
HSPA6	Sense	5′-GGCCATGACCAAGGACAACA-3′ (1760–1779)	NM_002155
	Antisense	5′-AACCATCCTCTCCACCTCCT-3′ (1976–1957)	
DNAJB1	Sense	5′-ACCCGGACAAGAACAAGGAG-3′ (135–154)	NM_006145
	Antisense	5′-GCCACCGAAGAACTCAGCAA-3′ (364–345)	
IDI1	Sense	5′-CACTAACCACCTCGACAAGC-3′ (304–323)	NM_004508
	Antisense	5′-CTTCTTGGTCTCAGCTCC-3′ (400–383)	
HMGCS1	Sense	5′-ACGGTATGCCCTGGTAGTTG-3′ (564–583)	NM_002130
	Antisense	5′-GCGGTCTAATGCACTGAGGT-3′ (807–788)	
RPS27A	Sense	5′-TTACGGGGAAGACCATCACC-3′ (61–80)	NM_002954
	Antisense	5′-CCACCACGAAGTCTCAACAC-3′ (265–246)	

BAG3, BCL2-associated athanogene 3; *DNAJB1*, DnaJ (Hsp40) homolog, subfmaily B, member 1; *HMGCS1*, 3-hydroxy-3-methylglutaryl–coenzyme A synthase 1; *HSPA1B*, heat shock 70 kDa protein 1B; *HSPA6*, heat shock 70 kDa protein 6; *IDI1*, isopentenyl-diphosphate delta isomerase; *RPS27A*, ribosomal protein S27a

quantitative PCR was performed by using the specific primers listed in Table 1. Temperature cycling conditions for each primer consisted of 10 min at 95 °C followed by 40 cycles for 30 s at 95 °C, 1 min at 60 °C and 1 min at 72 °C. The dissociation analysis was carried out over the range from 55 to 95 °C by monitoring SYBR Green fluorescence and PCR-specific products were determined as a single peak at the melting curves more than 80 °C. In addition, the specificity of primers was confirmed as a single band with the correctly amplified fragment size through an agarose gel electrophoresis of the real-time quantitative PCR products. Each mRNA expression level was normalized with respect to the mRNA expression of RPS27A.

2.10. Statistical analysis

Data are presented as means ± SD. Statistical analysis was carried out using Student's *t*-test and *P* values less than 0.05 were regarded as significant.

3. Results

3.1. Effects of ultrasonic intensity on cell viability and apoptosis in human leukemia Molt-4 cells

As shown in Fig. 2(A), the cell viability detected by trypan blue dye exclusion test 6 h after the low intensity pulsed US treatment (1 min) was significantly decreased at intensities more than 0.2 W/cm^2, with the cell viability of 88.4±9.3 (%), 79.8±8.5 and 44.2±6.2 at intensities of 0.3, 0.4 and 0.5 W/cm^2, respectively. On the other hand, the apoptosis detected by observing the DNA fragmentation assay 6 h after the low intensity pulsed US treatment (1 min) was significantly increased at intensities more than 0.2 W/cm^2, 24.0±3.3 (%), 26.0±4.6, and 26.5±2.4 at intensities of 0.3, 0.4 and 0.5 W/cm^2, respectively (Fig. 2(B)). Next, the relationship between ultrasonic intensity and free radical formation was studied using EPR-spin trapping with DMPO. The EPR signal of DMPO-OH adducts 1 min after the low intensity pulsed US treatment (1 min) was not detected up to 0.2 W/cm^2, and increased with increasing intensity up to 0.5 W/cm^2. The values of intensities of 0.3, 0.4 and 0.5 W/cm^2 were 0.015±0.01 (relative units), 0.044±0.023 and 0.059±0.022, respectively (Fig. 2(C)). During the sonication procedure, low intensity pulsed US at 0.3 W/cm^2 for 1 min slightly increased the temperature of medium 0.30±0.10 °C as measure by a digital thermometer (model 7563, Yokogawa Electric Co., Tokyo, Japan). Thus, we considered that thermal effect could be neglected in this US condition. Considering the effects of US on the basis of these data, we chose intensity of 0.3 W/cm^2 for the remainder of our studies.

3.2. Identification of genes responsive to low intensity pulsed ultrasound

To identify genes responsive to non-thermal low intensity pulsed US in the cells, we carried out DNA microarray analysis of cells cultured at 3 h after US treatment (for 1 min at 0.3 W/cm^2). Genes were considered up- or down-regulated, if each value and the average fold change were 1.5 or greater in two different experiments. Of approximately 16,600 genes

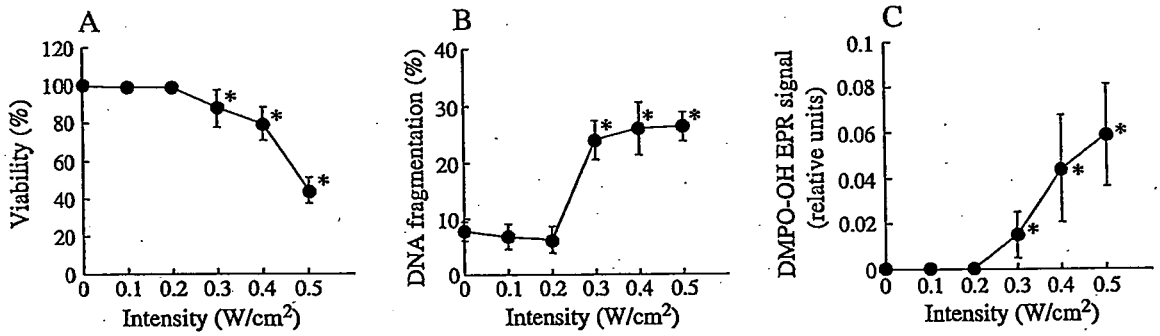

Fig. 2. The effects of ultrasonic intensity on cell viability (A), DNA fragmentation (B) and free radical formation induced by US (C). The cells were sonicated for 1 min at 0–0.5 W/cm^2, 1 MHz pulsed (10% DF, 100 Hz) and cultured at 37 °C. (A) After 6 h culture, the cell viability was evaluated by trypan blue dye exclusion test. (B) After 6 h culture, DNA fragmentation was assayed. (C) After 1 min culture, EPR-spin trapping with DMPO was employed to detect US generated free radicals. One unit of the *Y*-axis is calculated to correspond to about 19.0 μM of TEMPOL. Data indicate means ± SD for four different experiments. *$P < 0.05$ vs. control (intensity: 0 W/cm^2) (Student's *t*-test).

examined, four up-regulated genes, BCL2-associated athanogene 3 (*BAG3*), DnaJ (Hsp40) homolog, subfamily B, member 1 (*DNAJB1*), heat shock 70 kDa protein 1B (*HSPA1B*), and heat shock 70 kDa protein 6 (*HSPA6*), and two down-regulated genes, isopentenyl-diphosphate delta isomerase 1 (*IDI1*) and 3-hydroxy-3-methylglutaryl–coenzyme A synthase 1 (*HMGCS1*) were identified (Table 2). To verify the results of the microarray experiments, real-time quantitative PCR was performed. The results are summarized in Fig. 3. Although the expression levels of these genes were not completely comparable to that found by microarray analysis, the expression levels of *BAG3*, *DNAJB1*, *HSPA1B* and *HSPA6* were significantly increased, with expression levels being 6.3-, 3.3-, 7.3- and 311-fold, respectively. In contrast, the expression levels of *IDI1* and *HMGCS1* were significantly decreased, with the expression levels being 0.45 and 0.34-fold, respectively.

4. Discussion

US have been widely used for diagnosis and therapy in many medical fields. More recently, following a report by Lagneaux et al. [12], we also reported that non-thermal low intensity pulsed US treatment (1 MHz, 0.3 W/cm^2, 1 min) induced apoptosis in human leukemia cell lines such as U937, Jurkat and Molt-4 [9,22]. In addition, low intensity pulsed US have been shown to promote cell proliferation in human skin fibroblasts [25] and to stimulate cell proliferation and differentiation in human periosteal cells [26]. In the present study, non-thermal low intensity pulsed US induced apoptosis with minimal cell lysis and free radical formation was observed in human leukemia Molt-4 cells in the cases of our previous studies [9,22]. In addition, DNA microarray and real-time quantitative PCR analyses suggested that six genes showed changed levels of expression in US-treated Molt-4 cells. To our best knowledge, this is the first report of DNA microarray analysis of genes that are differentially expressed in response to apoptosis induced by non-thermal low intensity pulsed US in human leukemia cells. Of the approximately 16,600 genes analyzed, four genes including *BAG3*, *DNAJB1*, *HSPA1B* and *HSPA6* showed increased levels of expression while two genes including *IDI1* and *HMGCS1* showed decreased levels in Molt-4 cells 3 h after the US treatment. Of the four up-regulated genes, three heat shock proteins (HSPs), HSPA1B, HSPA6 and DNAJB1, were involved. HSPs are important modifying factors in cellular responses to a variety of physiological relevant conditions such as hyperthermia, oxidative stress, exercise and so on, and play important physiological roles for both normal cellular functions and survival after a stress [27]. HSPA1B and HSPA6 or DNAJB1 are isoforms of inducible Hsp70 or Hsp40, respectively. Inducible

Table 2
Up- and down-regulated genes after sonication in Molt-4 cells

Gene	Fold change			Genbank accession no.
	Exp. 1	Exp. 2	Average	
Up-regulated				
HSPA1B	1.9	1.5	1.7	NM_005346
BAG3	1.5	2.1	1.8	NM_004281
HSPA6	1.7	2.6	2.1	NM_002155
DNAJB1	2.2	2.9	2.6	NM_006145
Down-regulated				
IDI1	0.58	0.67	0.62	NM_004508
HMGCS1	0.52	0.66	0.59	NM_002130

Microarray analysis was performed. Details of experimental conditions described in Section 2.

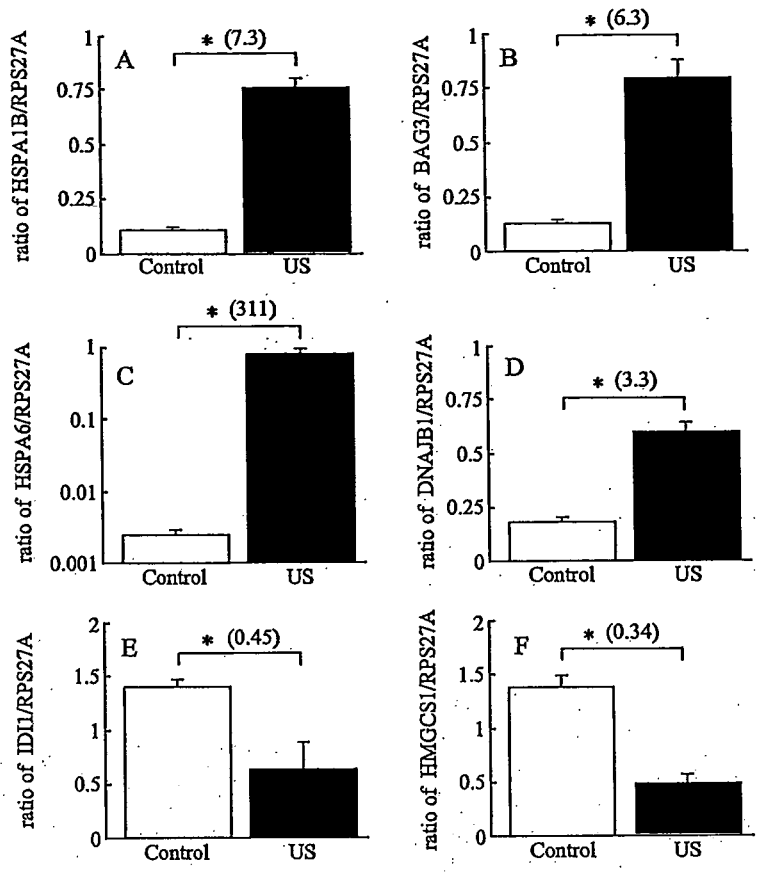

Fig. 3. Verification of the DNA microarray results with real-time quantitative PCR. The cells were exposed to US for 1 min at 0.3 W/cm^2, 1 MHz pulsed (10% DF, 100 Hz) and cultured for 3 h at 37 °C. Reverse transcriptase reaction was carried out with total RNA. Real-time quantitative PCR was performed according to the manufacture's instructions. mRNA level was normalized by *RPS27A*. A, *HSPA1B*; B, *BAG3*; C, *HSPA6*; D, *DNAJB1*; E, *IDI1* and F, *HMGCS1*. Data indicate means ± SD for four different experiments. *$P < 0.05$ vs. control (Student's t test).

Hsp70 and Hsp40 have been shown to protect cells from necrosis [28] and apoptosis [29,30] and co-operate with Hsp70 [31], respectively. It has been demonstrated that the anti-apoptotic activities of BAG-family proteins including BAG3 may be dependent on their interactions with Hsp70 and/or binding to Bcl-2, an anti-apoptotic protein [32,33]. Interestingly, in the present study, the expression of *BAG3* was significantly elevated in US-treated cells. We therefore speculate that *BAG3* and *Hsps*, *DNAJB1*, *HSPA1B* and *HSPA6*, may be up-regulated to protect cells from apoptosis. IntelliGene HS human Expression microarray used here is spotted with genes for 42 HSPs containing 11 Hsp70 and 21 Hsp40 proteins and four BAG-family proteins. However, only four genes out of 46 genes were increased in this experiment. The mechanisms by which low intensity pulsed US up-regulates these four genes and their physiological roles in US-treated cells remain a subject of further study.

In the present study, genes including IDI1 and HMGCS1 showed decreased levels of expression in the cells treated with US. Both HMGCS1 and IDI1 are enzymes in cholesterol biosynthesis, and the former drives the condensation of acetyl-CoA with acetoacetyl-CoA to form HMG-CoA and the latter catalyzes the rearrangement of isopentenyl diphosphate to its highly electrophilic isomer, dimethylallyl diphosphate [34,35]. It seems likely that the cholesterol biosynthesis pathway is down-regulated in apoptotic cells induced by US. Further studies will be necessary to clarify functions of these two genes in the apoptotic cells induced by low intensity pulsed US.

By using UniGEMV Ver2.0 human gene expression DNA microarrays to detect approximately 9200 genes, we previously demonstrated that five up-regulated genes (ferritin, heavy polypeptide 1, AU RNA-binding protein/enoyl–Coenzyme A hydratase, v-jun avian sarcoma virus 17 oncogene homolog, expressed

sequence tag (GenBank Accession number: N35555) and HO-1) and two down-regulated genes (v-myb avian myeloblastosis viral oncogene homolog and cathepsin G) were identified in the human lymphoma U937 cells at 6 h after exposure to fairly intense continuous waves (1 MHz, 4.9 W/cm^2, for 1 min) which induced significant cell lysis and free radicals [20]. Moreover, under nearly experimental condition, DNA microarray analysis indicated that PCTAIRE protein kinase 1 transcript variant 2 and HO-1 were up-regulated while leukemia inhibitory factor and chemokine ligand 10 were down-regulated by using IntelliGene II Human CHIP 1 DNA microarrays to detect approximately 3900 genes [21]. These microarray and real-time quantitative PCR results suggested that HO-1 is the most sensitive gene in U937 cells treated with low intensity continuous US [20,21]. However, all of these differentially expressed genes containing HO-1 were not identified in our present experiments using low intensity pulsed US. This discrepancy may be due to different experimental conditions such as the type of microarray, intensity of US and origin of the cell.

In conclusion, the present results will provide a basis for further understanding of the molecular mechanisms of biological effects of low intensity pulsed US. Here, we used the standing wave field induced by millisecond pulsed-ultrasound, and the detection of change of gene expression in the progressive wave field remains for further experiment.

Acknowledgements

The authors express their appreciation to Drs Shinichiro Umemura and Hideki Yoshikawa, Central Research Laboratory, Hitachi Co. Ltd, Tokyo, Japan for their support on measurement of peak pressure amplitude of the ultrasonic apparatus. This study is supported in part by the Grant in Aid for Scientific Research on Priority Areas (12217049) from the Ministry of Education, Culture, Sports, Sciences and Technology; in part by the 21st Century COE Program of the Toyama Medical and Pharmaceutical University, Japan; and also in part by Research and Development Committee Program of the Japan Society of Ultrasonics in Medicine.

References

[1] K.S. Suslick, Sonochemistry, Science 247 (1990) 1439–1445.
[2] P. Riesz, T. Kondo, Free radical formation induced by ultrasound and its biological implications, Free Radic. Biol. Med. 13 (1992) 247–270.
[3] L.B. Feril Jr., T. Kondo, Biological effects of low intensity ultrasound: the mechanism involved, and its implications on therapy and on biosafety of ultrasound, J. Radiat. Res. 45 (2004) 479–489.
[4] A. Abdollahi, S. Domhan, J.W. Jenne, M. Hallaj, G. Dell'Aqua, M. Mueckenthaler, et al., Apoptosis signals in lymphoblasts induced by focused ultrasound, Fed. Am. Soc. Exp. Biol. J. 18 (2004) 1413–1414.
[5] H. Ashush, L.A. Rozenszajn, M. Blass, M. Barda-Saad, D. Azimov, J. Radnay, et al., Apoptosis induction of human myeloid leukemic cells by ultrasound exposure, Cancer Res. 60 (2000) 1014–1020.
[6] L.B. Feril Jr., T. Kondo, Major factors involved in the inhibition of ultrasound-induced free radical production and cell killing by pre-sonication incubation or by high cell density, Ultrason. Sonochem. 12 (2005) 353–357.
[7] L.B. Feril Jr., T. Kondo, Q.L. Zhao, R. Ogawa, K. Tachibana, N. Kudo, et al., Enhancement of ultrasound-induced apoptosis and cell lysis by echo-contrast agents, Ultrasound Med. Biol. (2003) 331–337.
[8] L.B. Feril Jr., T. Kondo, K. Takaya, P. Riesz, Enhanced ultrasound-induced apoptosis and cell lysis by a hypotonic medium, Int. J. Radiat. Biol. 80 (2004) 165–175.
[9] L.B. Feril Jr., T. Kondo, Z.G. Cui, Y. Tabuchi, Q.L. Zhao, H. Ando, et al., Apoptosis induced by the sonomechanical effects of low intensity pulsed ultrasound in a human leukemia cell line, Cancer Lett. 221 (2005) 145–152.
[10] H. Honda, Q.L. Zhao, T. Kondo, Effects of dissolved gases and an echo contrast agent on apoptosis induced by ultrasound and its mechanism via the mitochondria-caspase pathway, Ultrasound Med. Biol. 28 (2002) 673–682.
[11] H. Honda, T. Kondo, Q.L. Zhao, L.B. Feril Jr., H. Kitagawa, Role of intracellular calcium ions and reactive oxygen species in apoptosis induced by ultrasound, Ultrasound Med. Biol. 30 (2004) 683–692.
[12] L. Lagneaux, E.C. de Meulenaer, A. Delforge, M. Dejeneffe, M. Massy, C. Moerman, et al., Ultrasonic low-energy treatment: a novel approach to induce apoptosis in human leukemic cells, Exp Hematol. 30 (2002) 1293–1301.
[13] A. Butte, The use and analysis of microarray data, Nat. Rev. Drug Discov. 1 (2002) 951–960.
[14] J. DeRisi, L. Penland, P.O. Brown, M.L. Bittner, P.S. Meltzer, M. Ray, et al., Use of a cDNA microarray to analyse gene expression patterns in human cancer, Nat. Genet. 14 (1996) 457–460.
[15] Y. Tabuchi, T. Kondo, M. Suzuki, M. Obinata, Genes involved in nonpermissive temperature-induced cell differentiation in Sertoli TTE3 cells bearing temperature-sensitive simian virus 40 large T-antigen, Biochem. Biophys. Res. Commun. 329 (2005) 947–956.
[16] Y. Tabuchi, Y. Arai, T. Kondo, N. Takeguchi, S. Asano, Identification of genes responsive to sodium butyrate in colonic epithelial cells, Biochem. Biophys. Res. Commun. 293 (2002) 1287–1294.
[17] Y. Tabuchi, T. Kondo, cDNA microarray analysis reveals chop-10 plays a key role in Sertoli cell injury induced by bisphenol A, Biochem. Biophys. Res. Commun. 305 (2003) 54–61.
[18] Y. Tabuchi, Q.L. Zhao, T. Kondo, DNA microarray analysis of differentially expressed genes responsive to bisphenol A, an alkylphenol derivative, in an in vitro mouse Sertoli cell model, Jpn. J. Pharmacol. 89 (2002) 413–416.

[19] H. Hirano, Y. Tabuchi, T. Kondo, Q.L. Zhao, R. Ogawa, Z.G. Cui, et al., Analysis of gene expression in apoptosis of human lymphoma U937 cells induced by heat shock and the effects of alpha-phenyl *N-tert*-butylnitrone (PBN) and its derivatives, Apoptosis 10 (2005) 331–340.

[20] Y. Tabuchi, T. Kondo, R. Ogawa, H. Mori, DNA microarray analyses of genes elicited by ultrasound in human U937 cells, Biochem. Biophys. Res. Commun. 290 (2002) 498–503.

[21] G. Kagiya, Y. Tabuchi, L.B. Feril, Jr., R. Ogawa, Q.L. Zhao, N. Kudo, et al., Confirmation of enhanced expression of heme oxygenase-1 gene induced by ultrasound and its mechanism: analysis by cDNA microarray system, real-time quantitative PCR, and western blotting, J. Med. Ultrasonics (in press).

[22] H. Ando, L.B. Feril, Jr., T. Kondo, Y. Tabuchi, R. Ogawa, Q.L. Zhao, et al., An echo-contrast agent, Levovist lowers the ultrasound intensity required to induce apoptosis of human leukemia cells, Cancer Lett., in press.

[23] K.S. Sellins, J.J. Cohen, Nuclear changes in the cytotoxic T lymphocyte-induced model of apoptosis, Immunol. Rev. 146 (1995) 241–266.

[24] P. Riesz, T. Kondo, C.M. Krishna, Free radical formation by ultrasound in aqueous solutions. A spin trapping study, Free Radic. Res. Commun. 10 (1990) 27–35.

[25] S. Zhou, A. Schmelz, T. Seufferlein, Y. Li, J. Zhao, M.G. Bachem, Molecular mechanisms of low intensity pulsed ultrasound in human skin fibroblasts, J. Biol. Chem. 279 (2004) 54463–54469.

[26] K.S. Leung, W.H. Cheung, C. Zhang, K.M. Lee, H.K. Lo, Low intensity pulsed ultrasound stimulates osteogenic activity of human periosteal cells, Clin. Orthop. Relat. Res. 418 (2004) 253–259.

[27] K.C. Kregel, Heat shock proteins: modifying factors in physiological stress responses and acquired thermotolerance, J. Appl. Physiol. 92 (2002) 2177–2186.

[28] J.A. Yaglom, D. Ekhterae, V.L. Gabai, M.Y. Sherman, Regulation of necrosis of H9c2 myogenic cells upon transient energy deprivation. Rapid deenergization of mitochondria precedes necrosis and is controlled by reactive oxygen species, stress kinase JNK, HSP72 and ARC, J. Biol. Chem. 278 (2003) 50483–50496.

[29] A. Saleh, S.M. Srinivasula, L. Balkir, P.D. Robbins, E.S. Alnemri, Negative regulation of the Apaf-1 apoptosome by Hsp70, Nat. Cell Biol. 2 (2000) 476–483.

[30] R. Steel, J.P. Doherty, K. Buzzard, N. Clemons, C.J. Hawkins, R.L. Anderson, Hsp72 inhibits apoptosis upstream of the mitochondria and not through interactions with Apaf-1, J. Biol. Chem. 279 (2004) 51490–51499.

[31] R. Kaneko, Y. Hayashi, I. Tohnai, M. Ueda, K. Ohtsuka, Hsp40 a possible indicator for thermotolerance of murine tumour in vivo, Int. J. Hyperthermia 13 (1997) 507–516.

[32] H. Doong, A. Vrailas, E.C. Kohn, What's in the 'BAG'?–A functional domain analysis of the BAG-family proteins, Cancer Lett. 188 (2002) 25–32.

[33] S. Takayama, Z. Xie, J.C. Reed, An evolutionarily conserved family of Hsp70/Hsc70 molecular chaperone regulators, J. Biol. Chem. 274 (1999) 781–786.

[34] F.M. Hahn, J.W. Xuan, A.F. Chambers, C.D. Poulter, Human isopentenyl diphosphate: dimethylallyl diphosphate isomerase: overproduction, purification, and characterization, Arch. Biochem. Biophys. 332 (1996) 30–34.

[35] D.J. Wilkin, S.Y. Kutsunai, P.A. Edwards, Isolation and sequence of the human farnesyl pyrophosphate synthetase cDNA. Coordinate regulation of the mRNAs for farnesyl pyrophosphate synthetase, 3-hydroxy-3-methylglutaryl coenzyme A reductase, and 3-hydroxy-3-methylglutaryl coenzyme A synthase by phorbol ester, J. Biol. Chem. 265 (1990) 4607–4614.

British Journal of Cancer (2007) 97, 170–176

www.bjcancer.com

Clinical Studies

A phase I and pharmacokinetic study of NK105, a paclitaxel-incorporating micellar nanoparticle formulation

T Hamaguchi*[,1], K Kato[1], H Yasui[1], C Morizane[1], M Ikeda[1], H Ueno[1], K Muro[1], Y Yamada[1], T Okusaka[1], K Shirao[1], Y Shimada[1], H Nakahama[2] and Y Matsumura[3]

[1]Department of Medicine National Cancer Center Hospital, 5-1-1 Tsukiji, Chuo-ku, Tokyo 104-0045, Japan; [2]Clinical Trial Coordinating Division, National Cancer Center Hospital, 5-1-1 Tsukiji, Chuo-ku, Tokyo 104-0045, Japan; [3]Investigative Treatment Division, Research Center for Innovative Oncology, National Cancer Center Hospital East, 6-5-1 Kashiwanoha, Kashiwa, 277-8577, Japan

This phase I study was designed to examine the maximum tolerated dose (MTD), the dose-limiting toxicities (DLTs), the recommended dose (RD) for phase II, and the pharmacokinetics of NK105, a new polymeric micelle carrier system for paclitaxel (PTX). NK105 was administered as a 1-h intravenous infusion every 3 weeks, without antiallergic premedication. The starting dose was 10 mg m^{-2}, and the dose was escalated according to the accelerated titration method. Nineteen patients were recruited. The tumour types treated included pancreatic ($n=11$), bile duct ($n=5$), gastric ($n=2$), and colonic ($n=1$) cancers. Neutropenia was the most common haematological toxicity. A grade 3 fever developed in one patient given 180 mg m^{-2}. No other grades 3 or 4 nonhaematological toxicities, including neuropathy, was observed during the entire study period. DLTs occurred in two patients given 180 mg m^{-2} (grade 4 neutropenia lasting for more than 5 days). Thus, this dose was designated as the MTD. Grade 2 hypersensitivity reactions developed in only one patient given 180 mg m^{-2}. A partial response was observed in one patient with pancreatic cancer. The maximum concentration (C_{max}) and area under the concentration (AUC) of NK105 were dose dependent. The plasma AUC of NK105 at 150 mg m^{-2} was approximately 15-fold higher than that of the conventional PTX formulation. NK105 was well tolerated, and the RD for the phase II study was determined to be 150 mg m^{-2} every 3 weeks. The results of this phase I study warrant further clinical evaluation.

British Journal of Cancer (2007) **97,** 170–176. doi:10.1038/sj.bjc.6603855 www.bjcancer.com
Published online 26 June 2007

Keywords: NK105; paclitaxel; polymer micelles; phase I study; DDS

Paclitaxel (PTX), an antimicrotubule agent, has a wide spectrum of antitumour activity including ovarian, breast, stomach, lung, and head and neck cancers (Rowinsky *et al*, 1990; Carney, 1996; Crown and O'Leary, 2000). The clinically used PTX preparation is a mixture of Cremophor EL and ethanol because of PTX's poor water solubility. However, the use of Cremophor EL is known to be associated with acute hypersensitivity reactions (Weiss *et al*, 1990; Rowinsky and Donehower, 1995; Kloover *et al*, 2004). Other PTX preparations that have been categorised as drug delivery systems (DDS) have also been developed. These preparations include Xyotax (polyglutamate-conjugated PTX; Singer *et al*, 2003; Boddy *et al*, 2005), Abraxane (PTX coated with albumin; Ibrahim *et al*, 2002; Deisai *et al*, 2003; Nyman *et al*, 2005), and Genexol-PM (a PTX micelle in which PTX has been simply solubilised; Kim *et al*, 2004). The common advantage shared by these formulations is that they are injectable intravenously without the mixture of Cremophor EL and ethanol. Among them, Abraxane has been approved for metastatic breast cancer by the Food and Drug Administration in the USA based on the results of a randomised phase 3 trial. In this trial, Abraxane demonstrated significantly higher response rates, compared with standard PTX, and a significantly longer time to progression (Gradishar *et al*, 2005). In addition, the incidence of grade 4 neutropenia was significantly lower for Abraxane than for PTX. However, peripheral sensory neuropathy was more common in the arm (Gradishar *et al*, 2005).

NK105 is a PTX-incorporating 'core-shell-type' polymeric micellar nanoparticle formulation (Hamaguchi *et al*, 2005). This particle can be injected intravenously without the use of Cremophor EL or ethanol as a vehicle. Therefore, NK105 is expected to possess a clinical advantage similar to that of the above-mentioned PTX formulations. The difference between NK105 and the other PTX dosage forms is that NK105 is expected to yield a markedly higher plasma and tumour area under the concentration (AUC), compared with those for the other PTX formulations. Moreover, regarding the toxic profiles, the repeated administration of NK105 to rats at 7-day intervals produced significantly fewer toxic effects on peripheral nerves than free PTX. Macromolecular drugs, including NK105, have been developed based on the characteristic macroscopic features of solid tumours, such as hypervasculature, the presence of vascular permeability factors stimulating extravasation within cancer, and the suppressed lymphatic clearance of macromolecules. These characteristics, which are unique to solid tumours, constitute the basis of the enhanced permeability and retention (EPR) effect (Matsumura and Maeda, 1986; Maeda *et al*, 2000; Duncan, 2003). The *in vivo*

*Correspondence: Dr T Hamaguchi; E-mail: thamaguc@ncc.go.jp
Received 13 March 2007; revised 23 May 2007; accepted 23 May 2007; published online 26 June 2007

antitumour activity of NK105 was significantly more potent than that of free PTX, probably because of enhanced tumour exposure through the EPR effect (Hamaguchi *et al*, 2005).

We conducted a phase I clinical trial using NK105 in patients with advanced solid tumours. The objectives of this trial were to determine the maximum tolerated dose (MTD), the phase II recommended dose (RD), and the pharmacokinetics of NK105.

PATIENTS AND METHODS

The protocol and all materials were approved by the Institutional Review Board of the National Cancer Center, Tokyo. This study was conducted in compliance with the Good Clinical Practice Guidelines of the International Conference on Harmonization and the Declaration of Helsinki Principles. Written informed consent was obtained from all the patients.

Therapeutic agent

NK105 was supplied by Nippon Kayaku Co. Ltd. (Tokyo, Japan) in 20-ml glass vials containing a dose equivalent to 30 mg of PTX. When reconstituted in 10 ml of 5% glucose solution and diluted with a total volume of 250 ml of 5% glucose, the reconstituted solution was stable for 24 h at room temperature. In our preclinical study, DLS and HPLC analysis showed that less than 2% of PTX incorporated in the micelles was released for 24 h at room temperature (data not shown).

Figure 1 shows the schematic structure of NK105, a PTX-entrapped polymeric micelle formulation. The NK105 polymers were constructed using polyethylene glycol (PEG) as the hydrophilic component and modified polyaspartate as the hydrophobic component. PEG is believed to form the outer shell of the micelle, producing a 'stealth' effect that enables NK105 to avoid being captured by the reticuloendothelial system.

The modified polyaspartate chain is hydrophobic and is believed to form the hydrophobic inner core of the micelles in aqueous media. The hydrophobic inner core enables NK105 to entrap a sufficient amount of PTX. NK105 has a diameter of about 90 nm (Hamaguchi *et al*, 2005).

Patients

Patients with solid tumours refractory to conventional chemotherapy and for whom no effective therapy was available were eligible for enrolment in this study, provided that the following criteria were met: a histologically confirmed malignant tumour; a performance status of $\leqslant 2$; an age of $\geqslant 20$ and <75 years; a normal haematological profile (neutrophil count $\geqslant 2000\,mm^{-3}$, platelet count $\geqslant 100\,000\,mm^{-3}$, hemoglobin $\geqslant 9\,g\,dl^{-1}$); normal hepatic function (total bilirubin level $\leqslant 1.5\,mg\,dl^{-1}$, AST and ALT $\leqslant 2.5$ times the upper normal limit); normal renal function (serum creatinine $\leqslant 1.5\,mg\,dl^{-1}$); normal cardiac function (New York Heart Association (NYHA) classification of $\leqslant 1$); normal pulmonary function ($PaO_2 \geqslant 60$ mm Hg); no chemotherapy within 4 weeks (6 weeks for nitrosourea or mitomycin C) of the administration of NK105; and a life expectancy of more than 2 months. Patients with serious infections (including hepatitis B, hepatitis C, or HIV) were ineligible for enrolment in the study. Patients who had been previously treated with a taxane were excluded because of assessing neuropathy. Patients were also excluded if they were pregnant or lactating. Additionally, any patient whom the investigators considered ineligible was excluded.

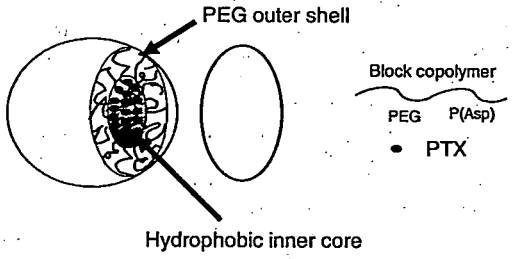

Figure 1 Schematic structure of NK105. A polymeric micelle carrier of NK105 consists of a block copolymer of PEG (molecular weight of about 12 000) and modified polyaspartate. PEG is believed to be the outer shell of the micelle. PEG is believed to form the outer shell of the micelle. NK105 has a highly hydrophobic inner core, and therefore can entrap a sufficient amount of PTX.

Drug administration

NK105 was dissolved in 5% glucose solution for injection at room temperature. NK105 was administered intravenously without in-line filtration and without premedication. NK105 solution was infused using an electric pump at a speed of $250\,ml\,h^{-1}$.

Dosage and dose escalation

The starting dosage of NK105 was $10\,mg\,m^{-2}$, which is one-third of the toxic dose low in dogs. NK105 was administered once every 3 weeks, and the treatment was continued unless a severe adverse event or disease progression was observed. Dose escalation was performed according to the previously described accelerated titration method (Simon *et al*, 1997; Matsumura *et al*, 2004).

Toxicity was graded from 1 to 4 using the National Cancer Institute Common Toxicity Criteria (version 2.0). Intrapatient dose escalation was not permitted. The MTD was defined as the level at which two out of six patients experienced dose-limiting toxicities (DLTs). The recommended dosage for a phase II trial was defined by the Efficacy and Safety Assessment Committee based on the safety, pharmacokinetics, and efficacy results of this trial. DLT was defined as grade 4 neutropenia lasting more than 5 days, a platelet count of less than $25\,000\,\mu l^{-1}$, or grade 3 or higher non-haematological toxicity, with the exception of nausea, vomiting, appetite loss, and hypersensitivity.

Pretreatment assessment and follow-up care

A complete medical history and physical examination, performance status evaluation, complete blood cell count (CBC), blood chemistry, urinalysis, electrocardiogram (ECG), and a computed tomography (CT) examination were performed in each patient. Other examinations were performed only in the presence of a specific clinical indication. Patients were physically examined every day until the second administration of NK105; CBC and blood chemistry tests were performed on day 3 and weekly thereafter. An ECG examination was repeated before each administration of NK105. Tumour marker levels were also measured before every administration. Tumour response was evaluated according to the Response Evaluation Criteria in Solid Tumors criteria (Therasse *et al*, 2000).

Liquid chromatography/tandem mass spectrometry determination of PTX concentrations

The PTX concentrations determined in the present phase I study represented the total drug concentrations (both micelle-entrapped and released). It was difficult to measure released PTX and micelle-entrapped PTX separately, because the equilibrium between both forms could not keep constant during the separating procedure. PTX was extracted from human plasma (0.2 ml) or urine (0.5 ml) by deproteinisation with acetonitrile. The quantifications of PTX in plasma and urine were performed using liquid chromatography/tandem mass spectrometry. Reversed-phase column-switching

chromatography was conducted using an ODS column and detection was enabled by electrospray ionisation of positive mode.

Pharmacokinetic analysis

The following pharmacokinetic parameters were calculated for each patient using a non-compartmental model using the WinNonlin Professional version 4.1 program (Pharsight Corporation, Mountain View, CA, USA). The maximum concentration (C_{max}) was the maximum observed plasma concentration of PTX, and the time-to-the-maximum concentration (T_{max}) was the time corresponding to C_{max}. The area under the concentration (AUC)–time curve from time zero up to the last quantifiable time point (AUC_{0-t}) was calculated using the linear trapezoidal rule, and the area under the concentration–time curve from zero until infinity ($AUC_{0-inf.}$) was calculated as the sum of AUC_{0-t} and the extrapolated area under the zero moment curve from the last quantifiable time point to infinity calculated by dividing the plasma concentration of the last quantifiable time point (observed value) by the elimination rate constant. The half-life of the terminal phase ($t_{1/2z}$) was calculated as $\log_e 2/\lambda z$, where λz is the elimination rate constant calculated from the terminal linear portion of the log of the concentration in plasma. Total clearance (CL_{tot}), the volume of distribution at steady state (V_{ss}), and renal clearance (CL_r) were calculated using the following equations, where D is the dose and $AUMC_{inf.}$ the area under the first moment curve from time zero until infinity:

$$CL_{tot} = D/AUC_{inf.}$$

$$V_{ss} = AUMC_{inf.}/AUC_{inf.} \times CL_{tot}$$

$$CL_r = \text{cumulative urinary excretion}/AUC_{inf.} / \text{body surface area}$$

RESULTS

Patient characteristics

Nineteen eligible patients were recruited for the study (Table 1). All the patients had received chemotherapy before enrolment. Prior therapies ranged from 1 to 3 regimens of chemotherapy. None of the patients had received taxane chemotherapy. All the patients were included in the safety and response analyses.

Dosing

Dosage escalation started at 10 mg m^{-2} and was increased up to 180 mg m^{-2}. In total, 73 administrations were performed in 19 patients. Eighteen patients received more than two administrations. The maximum number of treatments was 14 courses at 150 mg m^{-2}; the average number of administrations at all levels was 3.8 courses. Up until 80 mg m^{-2}, grade 2 toxicity was not observed during the first course.

According to the original protocol, the dosage of NK105 should have been doubled for each escalation until grade 2 toxicity. However, the safety committee recommended that the dosage should be raised by 40% instead of 100% at 110 mg m^{-2} and that a modified Fibonacci escalation method should be implemented. Therefore, we recruited three patients at dosage level 5 (110 mg m^{-2}) and re-started the dose identification study using a modified Fibonacci method.

Table 1 Patient characteristics

Number of patients	19
Male/female	13/6
Age (years)	
Median	57
Range	43–72
ECOG PS	
Median	0
0	10
1	9
Prior treatment	
Chemotherapy regimens	
Median	1
Range	1–3

Haematological toxicity

Significant myelosuppression was not observed up to level 4 (80 mg m^{-2}). At level 7 (180 mg m^{-2}), two out of five patients appeared to have acquired DLTs, namely grade 4 neutropenia lasting for more than 5 days. On the basis of these results, 180 mg m^{-2} was considered to be the MTD, with neutropenia as the DLT. Since a dosage of 150 mg m^{-2} was considered to be the recommended dosage for phase II studies, an additional four patients were enrolled at a dosage of 150 mg m^{-2}; one patient developed DLT, namely grade 4 neutropenia lasting for more than 5 days (Table 2). During the entire period of this study, G-CSF was never used to rescue patients.

Nonhaematological toxicity

The NK105 injection was generally uneventful and well tolerated in terms of nonhaematological toxicities (Table 2). Most of the toxicities were grade 1; none of the patients manifested grade 4 toxicity. A few patients developed a grade 1 elevation in AST or ALT, but these changes were transient. Pain or local toxicity in the area of the injection was not observed in any of the patients treated with NK105. No infusion-related reactions were observed; such reactions sometimes occur during liposomal drug administration. Patients were not premedicated with steroids or antihistamines. Only one patient at 180 mg m^{-2} developed grade 2 hypersensitivity. After the first course, the patient received premedication of hydrocortisone and did not develop such hypersensitivity after that. The other 18 patients did not experience any hypersensitivity during the study. Neuropathy occurred in a typical stocking/glove distribution and was manifested by numbness. Three patients at level 6 (150 mg m^{-2}) and three patients at level 7 (180 mg m^{-2}) experienced grade 1 neurotoxicity during 1 cycle. Of the four patients who received multicycle treatment more than five times, only three patients developed grade 2 neuropathy and the other patient developed grade 1 neuropathy. Even one patient who received 14 cycles of treatment experienced only grade 2 neuropathy.

Pharmacokinetics

The plasma concentrations of PTX after the intravenous infusion of NK105 were determined in each of the patients enrolled at a dose of 150 mg m^{-2} (Figure 2A). The C_{max} (Figure 2B) and AUC (Figure 2C) increased as the doses were escalated from 10 to 180 mg m^{-2}. The pharmacokinetic parameters are summarised in Table 3. The $t_{1/2z}$ ranged from 7.0 to 13.2 h, and a slight tendency towards a dose-dependent extension of this parameter was observed. The CL_{tot} ranged from 280.9 to 880.4 ml h^{-1} m^{-2}, and the V_{ss} ranged from 3668.9 to 10 400.3 ml m^{-2}. Although these parameters were slightly reduced depending on the dose, linear pharmacokinetics was assumed to have been observed in the dose range from 10 to 180 mg m^{-2}. The AUC of NK105 at 150 mg m^{-2} (recommended phase II dose) was about 15-fold larger than that of conventional PTX at dose of 210 mg m^{-2} (conventional dose for a

Table 2 Haematological and nonhaematological toxicities (cycle 1 and all cycles)

	10–110 mg m^{-2} (n=7) grade				150 mg m^{-2} (n=7) grade				180 mg m^{-2} (n=7) grade			
	1	2	3	4	1	2	3	4	1	2	3	4
Cycle 1												
Leukopenia	2	0	2	0	1	5	1	0	1	1	3	0
Neutropenia	1	0	1	1	0	2	1	3[a]	0	0	3	2[b]
Thrombocytopenia	1	0	0	0	2	0	0	0	4	0	0	0
Hemoglobin	1	0	0	0	2	2	0	0	1	0	0	0
Neuropathy	0	0	0	0	3	0	0	0	3	0	0	0
Myalgia	1	0	0	0	3	0	0	0	2	1	0	0
Arthralgia	1	0	0	0	4	0	0	0	3	0	0	0
Hypersensitivity	0	0	0	0	0	0	0	0	0	1	0	0
Rash	1	0	0	0	1	3	0	0	4	0	0	0
Fatigue	1	0	0	0	5	0	0	0	4	0	0	0
Fever	2	0	0	0	2	0	0	0	1	0	1	0
Anorexia	0	0	0	0	3	0	0	0	1	0	0	0
Nausea	1	0	0	0	1	0	0	0	1	0	0	0
Stomatitis	0	0	0	0	1	0	0	0	1	0	0	0
Alopecia	3	0	—	—	5	0	—	—	5	0	—	—
All cycles												
Leukopenia	3	0	2	0	1	4	2	0	1	1	3	0
Neutropenia	1	0	1	1	1	1	1	4	0	0	3	2
Thrombocytopenia	1	0	0	0	3	0	0	0	4	0	0	0
Hemoglobin	1	0	0	0	1	5	0	0	1	0	0	0
Neuropathy	2	0	0	0	1	3	0	0	4	0	0	0
Myalgia	1	1	0	0	3	0	0	0	2	1	0	0
Arthralgia	2	0	0	0	4	0	0	0	3	0	0	0
Hypersensitivity	0	0	0	0	0	0	0	0	0	1	0	0
Rash	1	0	0	0	3	3	0	0	4	0	0	0
Fatigue	3	0	0	0	5	1	0	0	4	0	0	0
Fever	3	0	0	0	3	1	0	0	1	0	1	0
Anorexia	2	1	0	0	2	1	0	0	2	0	0	0
Nausea	1	0	0	0	1	0	0	0	2	0	0	0
Stomatitis	1	0	0	0	2	0	0	0	1	0	0	0
Alopecia	2	2	—	—	4	3	—	—	4	1	—	—

[a]One of three patients developed DLT, namely grade 4 neutropenia lasting for more than 5 days. [b]These two patients developed DLT, namely grade 4 neutropenia lasting for more than 5 days.

3-week regimen in Japanese patients) (Tamura *et al*, 1995). The V_{ss} and CL_{tot} of NK105 were significantly lower than those of conventional PTX.

The cumulative urinary excretion rates of PTX (0–73 h) after the administration of NK105 were 2.8–9.2%. These values were low, similar to those reported after the administration of conventional PTX (Tamura *et al*, 1995). The CL_r ranged from 11.7 to 66.4 ml h^{-1} m^{-3}, and was slightly decreased with the dose. Since the ratio of CL_r to CL_{tot} was 3–9%, CL_r hardly contributed to CL_{tot}.

Therapeutic response

Six patients (two gastric, two bile duct, one colon, and one pancreatic) were evaluated as having had a stable disease for longer than 4 weeks at the time of the study's completion. A partial response was seen in a patient with metastatic pancreatic cancer who had been treated at 150 mg m^{-2}, and in whom the size of the liver metastasis had decreased by more than 90%, compared to the baseline scan (Figure 3A). This patient had previously undergone treatment with gemcitabine. The antitumour response was maintained for nearly 1 year. In a patient with stomach cancer who was treated at 150 mg m^{-2}, about 40% reduction was observed in a peritoneal metastasis, but a liver metastasis remained stable (Figure 3B).

DISCUSSION

The observed toxicities of NK105 were similar to those expected for conventional PTX. The DLT was neutropenia. The recommended phase II dose using a 3-week schedule was determined to be 150 mg m^{-2}. This recommended dose of NK105 is less than that of conventional PTX (210 mg m^{-2}). Since the plasma AUC of the recommended dose of NK105 was 15- to 20-fold higher than that of the recommended dose of conventional PTX (210 mg m^{-2}), whether the so-called therapeutic window of NK105 is wider than that of conventional PTX should be determined in a future phases II or III trial, although the therapeutic window of NK105 appears to be wider than that of free PTX in mice experiments (Hamaguchi *et al*, 2005).

In general, haematological toxicity was mild and well managed in this trial. PTX is known to cause cumulative peripheral neuropathy resulting in the discontinuation of treatment with PTX. At a dose of 150 mg m^{-2}, three out of seven patients experienced only grade 1 neuropathy during the first cycle. Since the patients enrolled in this trial had almost intractable cancer, such as pancreatic or stomach, a relatively small number of patients received multiple cycles of treatment. Therefore, NK105-related neurotoxicity could not be evaluated in this study. However, three out of four patients who received more than five cycles of treatment experienced transient grade 2 peripheral neuropathy, and other patient developed transient grade 1 peripheral neuropathy. Future phase II trials may clarify whether NK105 is less toxic in terms of peripheral neuropathy when compared with conventional PTX, Abraxane, and other PTX compounds. Another characteristic adverse effect of PTX is hypersensitivity, which may be mainly caused by Cremophor EL. Since NK105 is not formulated in a Cremophor EL-containing solvent, we presumed that hypersensitivity would be diminished.

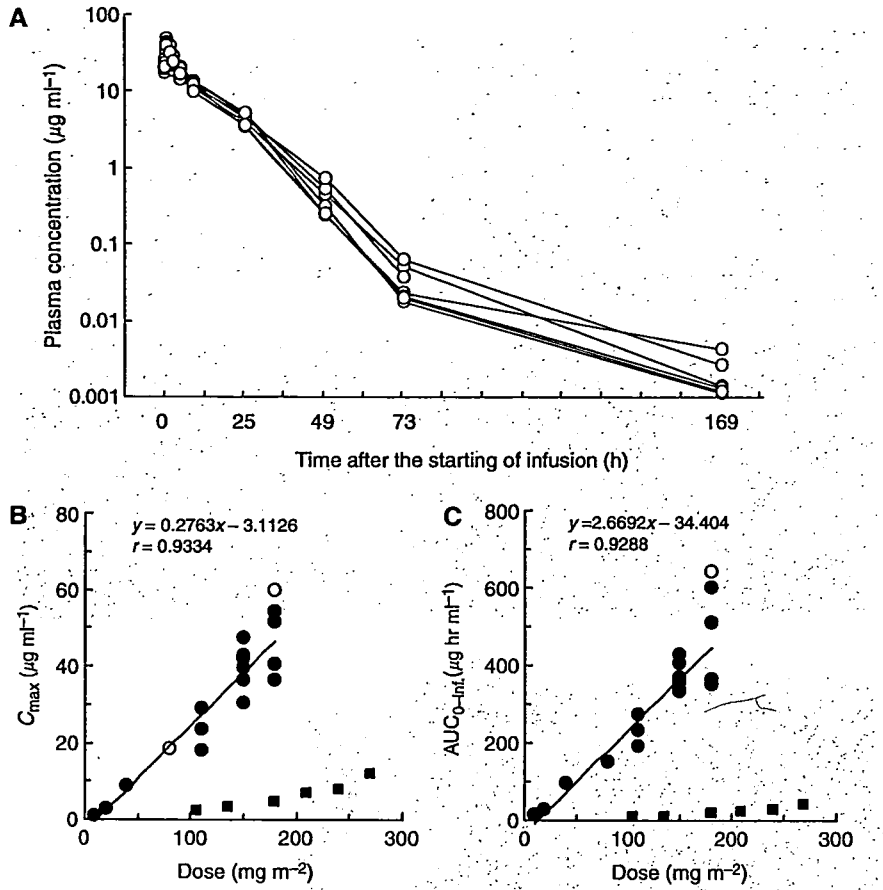

Figure 2 (**A**) Individual plasma concentrations of PTX in seven patients following 1-h intravenous infusion of NK105 at a dose of 150 mg m^{-2}. (**B**) Relationships between dose and C_{max}, and (**C**) between dose and $AUC_{0-inf.}$ of PTX in patients following 1-h intravenous infusion of NK105. Regression analysis for dose vs C_{max} was applied using all points except one patient at 80 mg m^{-2} whose medication time became 11 min longer and one patient at 180 mg m^{-2} who had medication discontinuation and steroid medication. (Plots were shown as open circle). Regression analysis for dose vs $AUC_{0-inf.}$ was applied using all points except one patient who had medication discontinuation and steroid medication. (Plot was shown as open circle.) Relationships between dose and C_{max}, and $AUC_{0-inf.}$ in patients following conventional PTX administration were plotted (closed square, see Tamura *et al*, 1995).

Table 3 Pharmacokinetic parameters

	Dose (mg m^{-2})	*n*	C_{max} (μg ml^{-1})	$AUC_{0-inf.}$ (μg h ml^{-1})	$t_{1/2}$ (h)	CL_{tot} (ml h^{-1} m^{-2})	V_{ss} (ml m^{-2})	UE[a] (%)	CL_r (ml h m^{-2})
NK105	10	1	0.9797	11.4	9	880.4	10400.3	7.5	66.4
	20	1	2.8971	29.1	8.5	687.9	8027	8.6	59.4
	40	1	8.8334	93.9	13.2	426.1	5389.8	5.2	22
	80	1	18.4533	149.3	7	535.8	5875.8	4.7	25.3
	110	3	23.3924	232	9.7	483.3	5881.2	7.6	35.6
			±5.6325	±39.1	±1.6	±82.7	±1512.0	±1.7	±6.9
	150	7	40.1699	369.8	10.6	408.6	4527.1	5.3	21.6
			±5.5334	±35.2	±1.3	±37.3	±639.5	±1.5	±6.5
	180	4[b]	45.6278	454.5	11.3	416.5	4983.4	5.9	23.7
			±8.6430	±119.1	±0.6	±104.7	±887.5	±1.4	±4.2

[a]UE, urinary excretion. [b]One patient at 180 mg m^{-2} level was omitted from the calculation of summary pharmacokinetic parameters, as there was administrating interruption for developing allergic reactions.

Indeed, the results of this clinical trial show that NK105 can be administered safely as a short infusion (1 h) without the administration of antiallergic agents like dexamethasone and antihistamine, although one patient at 180 mg m^{-2} developed transient grade 2 hypersensitivity at the first course. Therefore, NK105 may offer advantages in terms of safety and patient convenience and comfort.

The pharmacokinetic analysis of NK105 suggests that the distribution of PTX-incorporating micelles is mostly restricted to the plasma and, in part, to extracellular fluids in the body. This is consistent with data obtained in a preclinical study (Hamaguchi *et al*, 2005) showing that the distribution of NK105 in tissues is characterised by an EPR effect, similar to that of tumour and inflammatory lesions, or by the presence of a reticuloendothelial

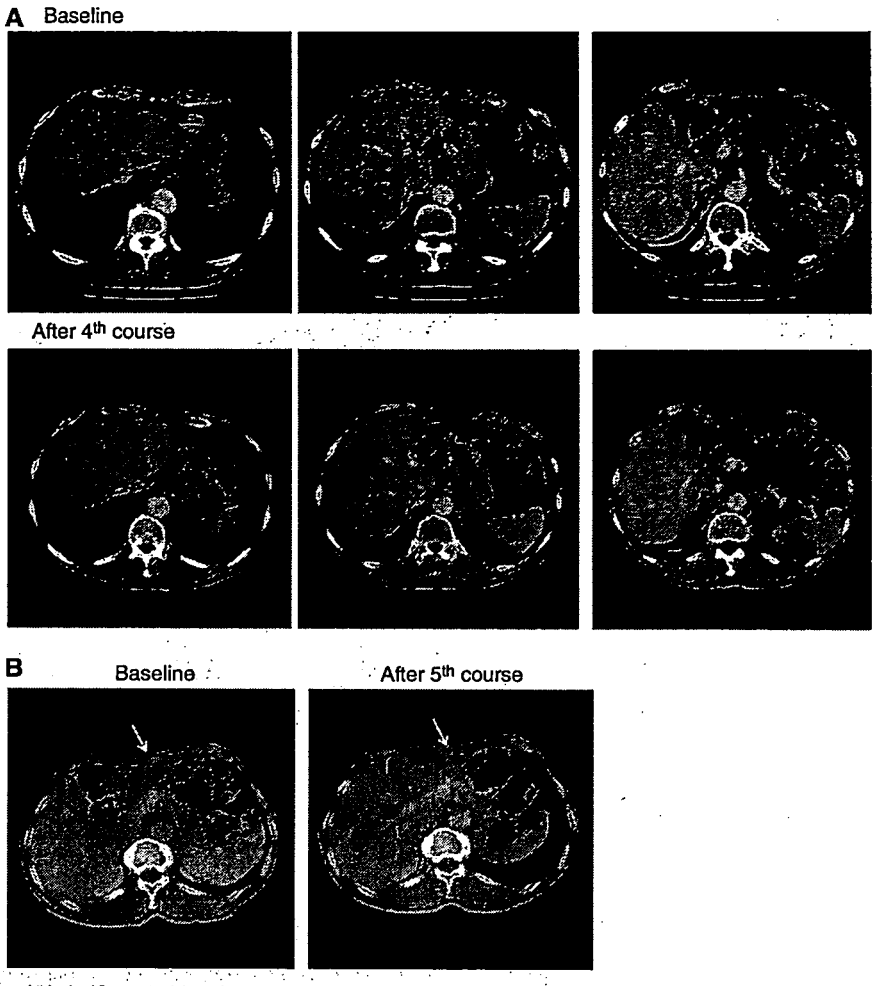

Figure 3 Serial CT scans. (**A**) A 60-year-old male with pancreatic cancer who was treated with NK105 at a dose level of 150 mg m^{-2}. Baseline scan (upper panels) showing multiple metastasis in the liver. Partial response, characterized by a more than 90% decrease in the size of the liver metastasis (lower panels) compared with the baseline scan. The antitumour response was maintained for nearly 1 year. (**B**) A 64-year-old male with stomach cancer who was treated with NK105 at a dose level of 150 mg m^{-2}. Baseline scan (left panel) showing a peritoneal metastasis and liver metastasis. About 40% reduction (right panel) was observed in peritoneal metastasis, but not in the liver metastasis after fifth course.

Table 4 Pharmacokinetic parameters

	Dose (mg m^{-2})	*n*	C_{max} (μg ml^{-1})	$AUC_{0-inf.}$ (μg h^{-1} ml^{-1})	$t_{1/2}$ (h)	CL_{tot} (ml h^{-1} m^{-2})	V_{ss} (ml m^{-2})	UE (%)	CL_r (ml h m^{-2})
NK105	150	7	40.1699 ±5.5334	369.8 ±35.2	10.6 ±1.3	408.6 ±37.3	4527.1 ±639.5	5.3 ±1.5	21.6 ±6.5
PTX	210	5	6.744 ±2.733	23.18 ±10.66	13.3 ±1.5	10740 ±4860	58900 ±24700	9.45 ±3.76	1020 ±648
XYOTAX[a]	233	4	NA	1583 ±572	120 ±28	276 ±63	6200 ±2100	NA	NA
Abraxane	300	5	13.52 ±0.95	17.61 ±3.70	14.6 ±2.04	17700 ±3894	370000 ±85100	NA	NA
Genoxol-PM	300	3	3.107 ±1.476	11.58 ±4.28	11.4 ±2.4	29300 ±13800	NA	NA	NA

[a]Conjugated taxanes.

system. When compared with conventional PTX at a dose of 210 mg m^{-2} (conventional dose for a 3-week regimen in Japanese patients), NK105 at a dose of 150 mg m^{-2} (recommended phase II dose) exhibited more than 15-fold larger plasma AUC and a 26-fold lower CL_{tot}. The larger plasma AUC is consistent with the stability of the micelle formulation in plasma. The V_{ss} of NK105 was 13-fold lower than that of conventional PTX. This suggests that PTX may have a relatively lower distribution in normal tissue, including normal neural tissue, following NK105 administration. Regarding the drug distribution in tumours, nanoparticle drug carriers have been known to preferentially accumulate in tumour tissues utilising the EPR effect (Matsumura and Maeda, 1986;

Maeda *et al*, 2000; Duncan, 2003). We speculate that NK105 accumulates more in tumour tissues than free PTX, since NK105 is very stable in the circulation and exhibits a markedly higher plasma AUC than free PTX. Moreover, a polymeric micelle carrier system for a drug has the potential to enable the sustained release of the drug inside a tumour following the accumulation of micelles in the tumour tissue (Hamaguchi *et al*, 2005; Uchino *et al*, 2005; Koizumi *et al*, 2006). Regarding NK105 in particular, this sustained release may begin at a PTX-equivalent dose of $<1\,\mu g\,ml^{-1}$ (data not shown). Consequently, the released PTX is distributed throughout the tumour tissue where it kills the cancer cells directly.

In the present study, NK105 appeared to exhibit characteristic pharmacokinetics different from those of other PTX formulations including conventional PTX, Abraxane, Genexol-PM, and Xyotax. For example, previous clinical PK data at each phase II recommended dose shown that plasma AUC and C_{max} were 11.58 and 3.1 in Genexol-PM (Table 4). The antitumour activities seen in two patients with intractable cancers are encouraging. In addition, we recently demonstrated in preclinical study that combined NK105 chemotherapy with radiation exerts a significantly more potent antitumour activity, compared with combined PTX therapy and radiation (Negishi *et al*, 2006). This data on NK105 justifies its continued clinical evaluation.

ACKNOWLEDGEMENTS

We thank the patients who participated in this trial. We also thank Kaoru Shiina and Hiromi Orita for their secretarial assistance.

REFERENCES

Boddy AV, Plummer ER, Todd R, Sludden J, Griffin M, Robson L, Cassidy J, Bissett D, Bernareggi A, Verrill MW, Calvert AH (2005) A phase I and pharmacokinetic study of paclitaxel poliglumex (XYOTAX), investigating both 3-weekly and 2-weekly schedules. *Clin Cancer Res* 11: 7834–7840

Carney DN (1996) Chemotherapy in the management of patients with inoperable non-small cell lung cancer. *Semin Oncol* 23: 71–75

Crown J, O'Leary M (2000) The taxanes: an update. *Lancet* 355: 1176–1178

Deisai N, Trieu V, Yao R (2003) Evidence of greater antitumor activity of Cremophor-free nanoparticle albumin-bound (nab) paclitaxel (Abraxane) compared to Taxol, role of a novel albumin transporter mechanism. *26th Annual San Antonio Breast Cancer Symposium* San Antonio, TX

Duncan R (2003) The dawning era of polymer therapeutics. *Nat Rev Drug Discov* 2: 347–360

Gradishar WJ, Tjulandin S, Davidson N, Shaw H, Desai N, Bhar P, Hawkins M, O'Shaughnessy J (2005) Phase III trial of nanoparticle albumin-bound paclitaxel compared with polyethylated castor oil-based paclitaxel in women with breast cancer. *J Clin Oncol* 23: 7794–7803

Hamaguchi T, Matsumura Y, Suzuki M, Shimizu K, Goda R, Nakamura I, Nakatomi I, Yokoyama M, Kataoka K, Kakizoe T (2005) NK105, a paclitaxel-incorporating micellar nanoparticle formulation, can extend *in vivo* antitumour activity and reduce the neurotoxicity of paclitaxel. *Br J Cancer* 92: 1240–1246

Ibrahim NK, Desai N, Legha S, Soon-Shiong P, Theriault RL, Rivera E, Esmaeli B, Ring SE, Bedikian A, Hortobagyi GN, Ellerhorst JA (2002) Phase I and pharmacokinetic study of ABI-007, a Cremophor-free, protein-stabilized, nanoparticle formulation of paclitaxel. *Clin Cancer Res* 8: 1038–1044

Kim TY, Kim DW, Chung JY, Shin SG, Kim SC, Heo DS, Kim NK, Bang YJ (2004) Phase I and pharmacokinetic study of Genexol-PM, a cremophor-free, polymeric micelle-formulated paclitaxel, in patients with advanced malignancies. *Clin Cancer Res* 10: 3708–3716

Kloover JS, den Bakker MA, Gelderblom H, van Meerbeeck JP (2004) Fatal outcome of a hypersensitivity reaction to paclitaxel: a critical review of premedication regimens. *Br J Cancer* 90: 304–305

Koizumi F, Kitagawa M, Negishi T, Onda T, Matsumoto S, Hamaguchi T, Matsumura Y (2006) Novel SN-38-incorporating polymeric micelles, NK012, eradicate vascular endothelial growth factor-secreting bulky tumors. *Cancer Res* 66: 10048–10056

Maeda H, Wu J, Sawa T, Matsumura Y, Hori K (2000) Tumor vascular permeability and the EPR effect in macromolecular therapeutics: a review. *J Control Release* 65: 271–284

Matsumura Y, Maeda H (1986) A new concept for macromolecular therapeutics in cancer chemotherapy: mechanism of tumoritropic accumulation of proteins and the antitumor agent smancs. *Cancer Res* 46: 6387–6392

Matsumura Y, Hamaguchi T, Ura T, Muro K, Yamada Y, Shimada Y, Shirao K, Okusaka T, Ueno H, Ikeda M, Watanabe N (2004) Phase I clinical trial and pharmacokinetic evaluation of NK911, a micelle-encapsulated doxorubicin. *Br J Cancer* 91: 1775–1781

Negishi T, Koizumi F, Uchino H, Kuroda J, Kawaguchi T, Naito S, Matsumura Y (2006) NK105, a paclitaxel-incorporating micellar nanoparticle, is a more potent radiosensitising agent compared to free paclitaxel. *Br J Cancer* 95: 601–606

Nyman DW, Campbell KJ, Hersh E, Long K, Richardson K, Trieu V, Desai N, Hawkins MJ, Von Hoff DD (2005) Phase I and pharmacokinetics trial of ABI-007, a novel nanoparticle formulation of paclitaxel in patients with advanced nonhematologic malignancies. *J Clin Oncol* 23: 7785–7793

Rowinsky EK, Donehower RC (1995) Paclitaxel (taxol). *New Engl J Med* 332: 1004–1014

Rowinsky EK, Cazenave LA, Donehower RC (1990) Taxol: a novel investigational antimicrotubule agent. *J Natl Cancer Inst* 82: 1247–1259

Simon R, Freidlin B, Rubinstein L, Arbuck SG, Collins J, Christian MC (1997) Accelerated titration designs for phase I clinical trials in oncology. *J Natl Cancer Inst* 89: 1138–1147

Singer JW, Baker B, De Vries P, Kumar A, Shaffer S, Vawter E, Bolton M, Garzone P (2003) Poly-(L)-glutamic acid-paclitaxel (CT-2103) [XYOTAX]; a biodegradable polymeric drug conjugate: characterization, preclinical pharmacology, and preliminary clinical data. *Adv Exp Med Biol* 519: 81–99

Tamura T, Sasaki Y, Nishiwaki Y, Saijo N (1995) Phase I study of paclitaxel by three-hour infusion: hypotension just after infusion is one of the major dose-limiting toxicities. *Jpn J Cancer Res* 86: 1203–1209

Therasse P, Arbuck SG, Eisenhauer EA, Wanders J, Kaplan RS, Rubinstein L, Verweij J, Van Glabbeke M, van Oosterom AT, Christian MC, Gwyther SG (2000) New guidelines to evaluate the response to treatment in solid tumors. European Organization for Research and Treatment of Cancer, National Cancer Institute of the United States, National Cancer Institute of Canada. *J Natl Cancer Inst* 92: 205–216

Uchino H, Matsumura Y, Negishi T, Koizumi F, Hayashi T, Honda T, Nishiyama N, Kataoka K, Naito S, Kakizoe T (2005) Cisplatin-incorporating polymeric micelles (NC-6004) can reduce nephrotoxicity and neurotoxicity of cisplatin in rats. *Br J Cancer* 93: 678–687

Weiss RB, Donehower RC, Wiernik PH, Ohnuma T, Gralla RJ, Trump DL, Baker Jr JR, Van Echo DA, Von Hoff DD, Leyland-Jones B (1990) Hypersensitivity reactions from taxol. *J Clin Oncol* 8: 1263–1268